Colloids and Surfaces A: Physicochemical and Engineering Aspects 652 (2022) 129927

Contents lists available at ScienceDirect

Colloids and Surfaces A: Physicochemical and Engineering Aspects

journal homepage: www.elsevier.com/locate/colsurfa

Rheology of saturated micellar networks: Wormlike micellar solutions vs. bicontinuous micellar phases

Teodora N. Stancheva, Mihail T. Georgiev, Gergana M. Radulova, Krassimir D. Danov *, Krastanka G. Marinova

Department of Chemical & Pharmaceutical Engineering, Faculty of Chemistry & Pharmacy, Sofia University, 1164 Sofia, Bulgaria

GRAPHICAL ABSTRACT

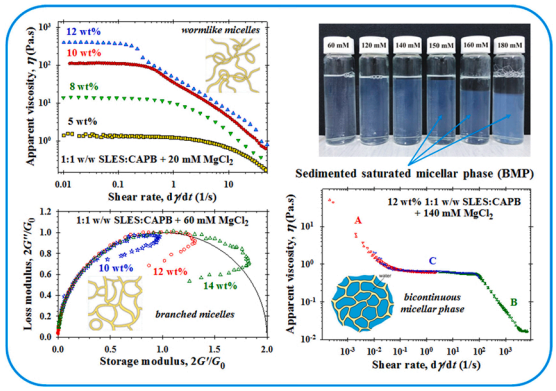

ARTICLE INFO

Keywords:
Wormlike micelles
Multiconnected micelles
Bicontinuous micellar phases
Micelles with divalent ions
Rheology of complex fluid

ABSTRACT

The subject of this work is to investigate the rheological behavior of mixed micellar solutions (sodium laurylethersulfate and cocamidopropyl betaine) in the presence of Mg^{2+} divalent counterions. With the rise of salt concentration, the viscosity of micellar solutions increases to a high maximum followed by a steep decrease because of the initial growth and entanglement of wormlike micelles and a subsequent transition to branched micelles forming of a saturated micellar network. The proposed systematic rheological measurements show considerable variations in the rheological responses of the solutions when increasing the salt concentration. Rheological behavior and data are used to distinguish the micellar phases and to study the relation to micellar structures. The wormlike micellar solutions have a typical shear thinning behavior with a well-defined zero-shear viscosity, η_0, described by the Cates reptation-reaction model or the augmented Maxwell model. Our data show that the power law dependence of η_0 on the surfactant concentration is stronger than that reported in the literature and it is influenced of the added electrolytes. The branched micellar structures are characterized by the lower viscosities and larger elasticities, which follow the Maxwell model up to the intermediate values of the frequency of oscillations, however peculiar deviations from the Cole-Cole plot at large frequencies are detected. The isolated bicontinuous micellar phases are Newtonian fluids with viscosity 0.4–0.7 Pa.s independent on the salt concentration up to high shear rates. The threshold salt concentration ensuring the onset of the bicontinuous

* Corresponding author.
E-mail address: KD@LCPE.Uni-Sofia.BG (K.D. Danov).

https://doi.org/10.1016/j.colsurfa.2022.129927
Received 5 June 2022; Received in revised form 2 August 2022; Accepted 8 August 2022
Available online 10 August 2022

micellar phase is described by a simple empirical rule. These phases are characterized by large elasticities and not negligible yield stresses. The property of the bicontinuous micellar phases to form spontaneously oil-in-water nanoemulsions could find applications in drug delivery, extraction and separation processes, pharmaceutics production, etc.

1. Introduction

The formation of large wormlike micelles is most frequently observed in mixed surfactant solutions (anionic and cationic; ionic and zwitterionic) [1–8] and in systems containing ionic surfactants and salts [5,7,9–12]. The apparent viscosity of the micellar solutions containing ionic surfactants increases to a high maximum with the rise of concentration of the added salt [7,10,13,14] because of the initial growth and entanglement of the wormlike micelles. The high viscosity of these concentrated and internally structured solutions is a result of various processes and interactions: hydrodynamic interactions [15,16]; relaxation mechanisms for long linear aggregates with reptation related to the curvilinear diffusion [17]; micelle reversible scission and end-interchange processes [18–21]. The Cates reptation-reaction model predicts correctly the variations of zero-shear viscosity, elasticity, relaxation, breakage and reptation times of wormlike micellar solutions for not large deviations from the Maxwell model [7,22,23]. Large deviations from the Maxwell model are not exceptions and for them, the augmented Maxwell model [7] gives information about the mean elasticity, viscosity and characteristic frequency of the micellar solutions. The power law dependence between the zero-shear viscosity and the total surfactant concentration with a power law index in the range from 3 to 3.5 is reported in the literature [10,24].

The peak of the so-called salt curves is a result of the transition from wormlike micelles to branched micelles. The screening of the electrostatic repulsion between the surfactant headgroups with salt concentration leads to the initial growth of spherocylindrical micelles, whereas the subsequent transition to branched aggregates can be explained in terms of the interfacial bending energy [24–27]. To the right of the peak, the decrease of the viscosity with the increase of the salt concentration is due to the formation of mobile junctions that can slide along the linear micelles [21, 28–31]. For branched micellar solutions, the viscosity depends on the total surfactant concentration as a power law with index from 1 to 2.5 [10,24]. The formation of saturated micellar network with the subsequent increase of the salt concentration has been used as an explanation of the rheological response of numerous experimental systems [6,24,32–36]. At a high salt concentration, the viscosity drops because of the phase separation due to the salting out of surfactant.

The formation of branched micelles and large multiconnected domains has been reported for various systems (ionic surfactants and their mixtures at high salt concentrations, nonionic surfactants upon the rise of temperature close to the cloud point, alkyl glycosides with the rise of surfactant concentration) [37–52]. In the literature, the terms “multiconnected micellar network” [24], “saturated network” [28] and “bicontinuous phase” [38,39,52] are used as synonyms. A phase separation of saturated micellar networks is established in mixed solutions of sodium laurylethersulfate (SLES) and cocamidopropyl betaine (CAPB) in the presence of divalent counterions (Ca^{2+}, Zn^{2+} and Mg^{2+}) [52]. In the case of added Mg^{2+} counterions, the sedimented drops coalesce and form a separate phase with a significant nanoemulsification capacity in the presence of small organic molecules. The cross-polarized light microscopy and the small-angle X-ray scattering experiments [52] identify the separated phase as *saturated micellar network* with a *bicontinuous structure* called below the bicontinuous micellar phase (BMP). The different specific binding of the Ca^{2+}, Mg^{2+} and Zn^{2+} ions to the headgroups of SLES leads to the considerable different phase behavior of micellar solutions. In the presence of Ca^{2+} counterions, the absolute value of the measured zeta potential of drops is high enough to prevent the coalescence of drops and the BMP does not form [52]. The addition of Zn^{2+} counterions leads to the lowest zeta potential by magnitude and simultaneous appearance of drops and crystallites [52]. The formation of separate BMF was observed only in the presence of Mg^{2+} ions: the drop coalescence is a result of specific ability of the magnesium ions to interact with the surfactant headgroups, to bridge between neighboring drops and promote their merging in a separate BMP.

In the present study, we investigate the rheological properties of CAPB+SLES micellar solutions in the presence of Mg^{2+} counterions for a wide range of surfactant and salt concentrations. Advanced rheology measurements and adequate theoretical interpretations help us to describe and distinguish the different regions, e.g. wormlike micellar solutions, branched micelles, formation of droplets of saturated micellar network, salting out of the surfactants at a high salt concentration (Section 3). The model parameters (zero-shear viscosity, elasticity, different relaxation times, characteristic frequency) for wormlike and branched micellar solutions are presented in Section 4. The detailed rheological study of the isolated saturated micellar networks (BMP) shows their unique properties, which are independent on the surfactant and salt concentrations of the solutions from which the BMPs are separated (Section 5). The main conclusions are summarized in Section 6.

2. Materials and methods

2.1. Materials

In our study, we used the anionic surfactant sodium laurylethersulfate with one ethylene oxide group (briefly SLES) with a molecular mass of 332.4 g/mol, a product of Stepan Co (commercial name STEOL CS-170). The critical micelle concentration (CMC) of SLES is 0.7 mM. The used zwitterionic surfactant was cocamidopropyl betaine (CAPB) with a mean molecular mass of 356 g/mol, a product of Evonic Nutrition & Care, GmbH Germany, under the trade name TEGO Betain F50. The CMC of CAPB is 0.089 mM and we established that 100 mM of CAPB contains an admixture of 118 ± 6 mM NaCl [7,53]. The used salts were $MgCl_2$ and $MgSO_4$, products of Merck (Germany).

At a fixed 1:1 wt ratio of the anionic and zwitterion surfactants, we studied the effect of the total surfactant concentration, C_{tot}, and of the added salt concentration, C_{salt}, on the rheological properties of the micellar solutions.

All solutions were prepared with deionized water purified by Elix 3 water purification system (Millipore) with a conductivity of 0.067 μS/cm. First, we prepared the stock binary surfactant solution by gentle stirring at room temperature. Second, the necessary amount of salt ($MgCl_2$ or $MgSO_4$) was dissolved by vigorous agitation on a temperature-controlled magnetic stirrer for 1 h at 60 °C. All measurements were carried out after overnight equilibration of the solution at 25 °C. The natural pH of all solutions was in the range from 5 to 6, so CAPB is in its zwitterionic form. At large enough salt concentrations (see Appendix A), the micellar solutions are transparent with small dispersed droplets. Upon sedimentation at the bottom of the vial, these drops spontaneously coalesce and form a separate phase. After 1 day of rest, single phase at the bottom of the vials (see Figs. A2–A7) was clearly seen, and this phase was identified as bicontinuous micellar phase [52]. Samples of the sediment (BMP) were further isolated and their rheological behavior was also studied and described, see Section 5.

Note that because of SLES dissociation and NaCl admixture in the CAPB samples, the amounts of Na^+ and Cl^- ions (ionic strength of the solutions) increase with the total surfactant concentration: for $C_{tot} = 5$

wt%, the solution contains 158 mM Na^+ and 83 mM Cl^- ions; for C_{tot} = 14 wt%, the respective solution contains 443 mM Na^+ and 232 mM Cl^- ions (see Table A1). The addition of a given concentration of $MgCl_2$ or $MgSO_4$ at a fixed C_{tot} produces a more pronounced relative change of the ionic strength for lower surfactant concentrations than that for the higher values of C_{tot}.

2.2. Experimental methods and protocols

The rheology of micellar solutions was measured by a rotational rheometer Bohlin Gemini (Malvern Instruments, UK) at $T = 25$ °C. The temperature was controlled by a Peltier element and the evaporation was suppressed by a solvent trap. The relative experimental error was less than 1%. To confirm the reproducibility of the obtained data, each rheological experiment was repeated at least three times starting with a newly prepared sample. In this case, the relative reproducibility measurement error increases and it was less than 5%.

We used three different working elements (appendix B) in order to inspect the rheological responses upon wide ranges of variation of the shear strains, γ, and their rates, $\dot{\gamma} \equiv d\gamma/dt$, shear stresses, τ, and frequencies of oscillations, ω. The first element (CP 2/60) defines a cone-and-plate geometry with: cone angle 2° minimal gap distance 70 μm; diameter 60 mm. This element was used for systematic measurements in all rheological regimes. The element PP 40 (parallel plate geometry) with the gap distance 1 mm and the diameter 40 mm was used to study the yield stress of the BMPs. The shearing surfaces were covered by sandpaper to check the wall slips effect. In contrast to PP 40, the Vane element (Appendix B) ensures a slippage of the boundary layer around the rotational element and produces considerably different shear strains vs. shear stresses experimental dependencies.

The apparent viscosity, $\eta \equiv \tau/\dot{\gamma}$, was measured in a steady shear regime as a function of the shear rate in a wide region of $\dot{\gamma}$ – from 0.01 to 100 s^{-1}. Depending on the surfactant and salt concentrations, two different types of η–vs.–$\dot{\gamma}$ dependencies (*flow curves*) were observed (e.g. Figs. 1a and 1b and Appendix C). For the regular flow curves (Fig. 1a), the apparent viscosity is constant at low shear rates (quasi-Newtonian behavior), so the mean constant viscosity in the plateau region defines the zero-shear viscosity, η_0. For higher shear rates, the apparent viscosity decreases with the rise of $\dot{\gamma}$ according to power law $\eta = \eta_{100}(\dot{\gamma}/100)^{-n}$, where the values of the power law index, n, are close to 1 and η_{100} is the most probable value of the viscosity at high shear rates $\dot{\gamma} = 100 s^{-1}$ [7]. In the case of irregular flow curves (Fig. 1b), the shear thinning regime starts from the lowest experimental shear rates. We used the analogous power law, $\eta = \eta_{0.01}(\dot{\gamma}/0.01)^{-n}$, to obtain the most probable value of viscosity, $\eta_{0.01}$, at low shear rates $\dot{\gamma} = 0.01 s^{-1}$. The power law indexes are again around 1. In the irregular regime, the viscosity is constant at high shear rates (Newtonian regime) and the mean value defines the Newtonian viscosity, η_∞.

In the *oscillatory regime*, the applied strain oscillates with given frequency ω and amplitude γ_a and a Fourier analysis is applied to calculate the storage, G', and loss, G'', moduli (see Figs. 1c and 1d and Appendix D). Generally, for nonlinear rheological systems [54], the moduli are complex functions of the frequency and amplitude of oscillations, $G' = G'(\omega, \gamma_a)$ and $G'' = G''(\omega, \gamma_a)$. For constant value of ω, the dependence of the moduli on the amplitude (Fig. 1d) has plateau for low amplitudes – the constant values, $G'(\omega) = G'(\omega, 0)$ and $G''(\omega) = G''(\omega, 0)$, define the

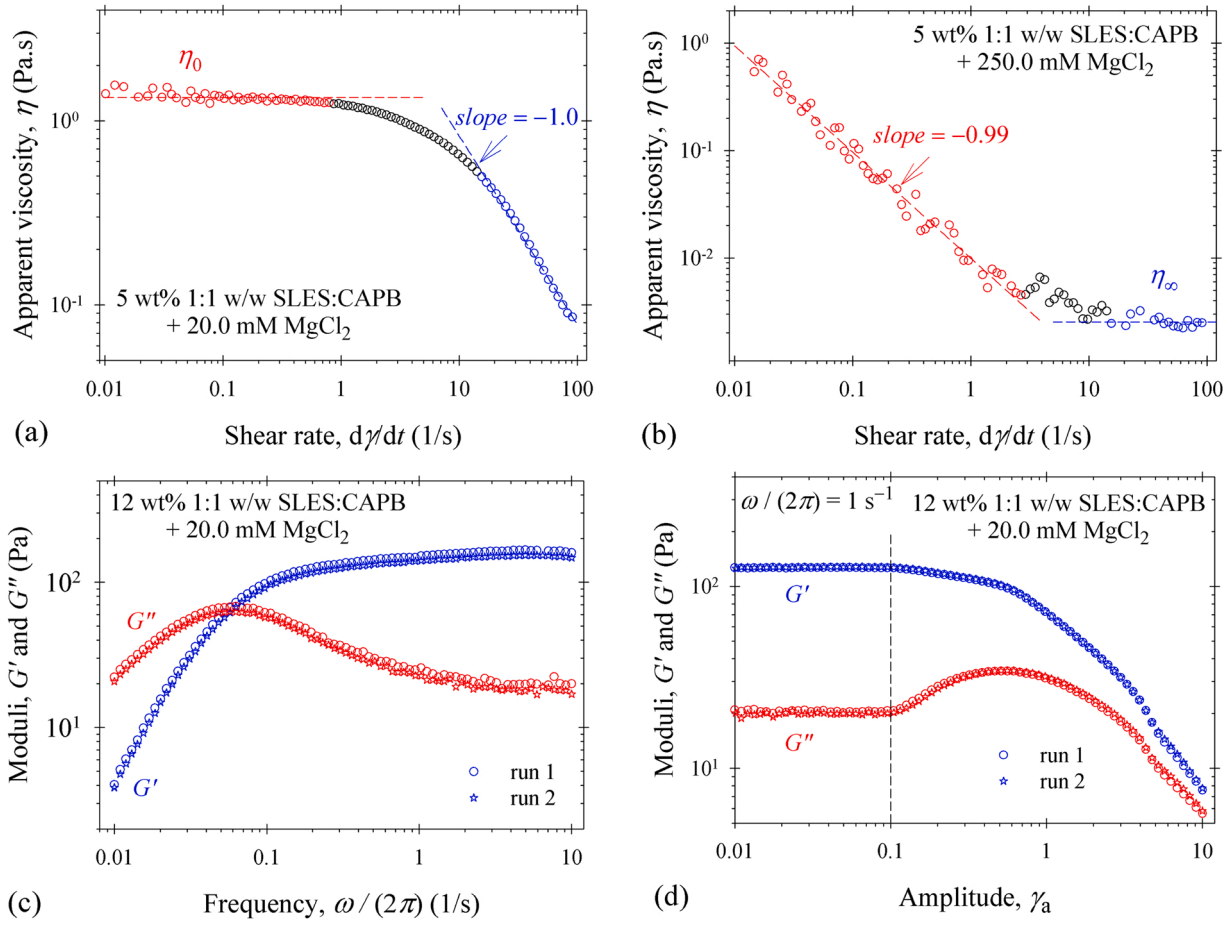

Fig. 1. Typical experimental raw data: flow curves for C_{tot} = 5 wt% in the presence of 20 mM $MgCl_2$ (a) and of 250 mM $MgCl_2$ (b); storage, G', and loss, G'', moduli obtained from oscillatory regime for C_{tot} = 12 wt% in the presence of 20 mM $MgCl_2$ vs. the frequency of oscillations for γ_a = 2% (c) and vs. the amplitude of the applied shear strain for $\omega/(2\pi) < 1 s^{-1}$ (d).

linear rheological regime with respect to the magnitude of the applied shear strain. One sees in Fig. 1d that the linear rheological response takes place for $\gamma_a < 10\%$. All oscillatory experiments, e.g. moduli–vs.–frequency (Fig. 1c), were performed up to high frequencies $\omega/(2\pi) \leq 100 s^{-1}$, but the linearity of the rheological response failed down at lower frequencies, even for $\gamma_a = 2\%$. For example, the linearity range is at $\omega/(2\pi) < 10 s^{-1}$ in Fig. 1c. All data processing for $G'(\omega)$ and $G''(\omega)$ determination and the obtained model parameters in Section 4 correspond to a linear rheological response of the studied systems.

To characterize the yield stress of the separated BMP, the rheological experiments were performed in the *stress-ramp regime*. The applied shear stress, τ, increases in a logarithmic scale from 0.01 to 100 Pa for a given time, t, and the shear strain, γ, is measured (Fig. 2a). A steep increase of γ is detected for $\tau > 10$ Pa. To ensure a stronger increase of the shear strain, the γ–vs.–τ curve is measured also in the case of a linear change of τ with time from 1 to 100 for 200 s (Fig. 2b). Fig. 2b shows that the shear strain increases several orders of magnitude up to 5×10^5 when applying this regime. A steep increase of γ is obtained for $\tau > 50$ Pa. These kinds of experiments were performed using all working elements (see Appendix B) in order to obtain adequate information on the effects of the shear volume and wall slip on the yield stress of bicontinuous micellar phases (Section 5).

3. Rheology of micellar solutions in a steady-shear regime

The rheological behavior of all micellar solutions in a steady-shear regime, η–vs.–$\dot{\gamma}$, was studied after gentle stirring of the solutions in order to re-disperse the sedimented drops or formed crystals, especially at large concentrations of added salt (Appendix A). For example, at $C_{tot} = 5$ wt%, the sedimentation of drops is observed for 50 mM $< C_{salt} \leq 150$ mM in the case of added $MgCl_2$ and for 90 mM $< C_{salt} \leq 150$ mM in the case of added $MgSO_4$ (cf. Figs. A3 and A8). The crystal formation because of the salting-out effect is detected for $C_{salt} > 150$ mM (see Fig. A9 in Appendix A). The determined viscosities (η_0, $\eta_{0.01}$, η_∞, and η_{100}) as a function of the concentration of Mg^{2+} are presented in Fig. 3 for $C_{tot} = 5$ wt% (see also Appendix C).

As seen in Fig. 3a for $C_{salt} < 20$ mM, the shear thinning takes place even for the lowest shear rates, $\dot{\gamma} = 0.01 s^{-1}$, and $\eta_{0.01}$ increases with C_{salt}, which indicates the growth of the spherocylindrical micelles [27]. These micelles are stable upon high shear rates (Fig. 3b) as evidenced by the increase of the Newtonian viscosity, η_∞, from 0.01 to 0.05 Pa.s. The steep rise of the zero-shear viscosity, η_0, up to 100 Pa.s is measured in the narrow region of added salt concentrations, 20 mM $\leq C_{salt} < 32$ mM, which is independent on the types of coions. The formed wormlike micellar structures become quite stable and the Newtonian regime is not reached even at $\dot{\gamma} = 100 s^{-1}$ – for that reason, viscosities η_{100} are of the order of 0.1 Pa.s (Fig. 3b).

The rheological measurements are a sensitive method for the precise determination of the transition from wormlike micelles to branched micelles (the right branches of the salt curves in Fig. 3a). The measured zero-shear viscosity decreases more than two orders of magnitude with the increase of the salt concentration up to the formation of droplets from saturated micellar network. The presence of crystals in the solutions leads to the increase of $\eta_{0.01}$ and the Newtonian viscosity η_∞.

With the rise of the total surfactant concentration, the size of spherocylindrical micelles increases as a square root of C_{tot} [27,55–57]. In contrast, Fig. 4a shows that the zero-shear viscosity of wormlike micellar solutions for a fixed $MgCl_2$ concentration, $C_{salt} \leq 30$ mM, increases orders of magnitude with C_{tot}. This effect is more pronounced for the lower added $MgCl_2$ concentrations. Note that the CAPB sample contains considerable amount of NaCl (Appendix A), which leads to the pronounced increase of the ionic strength with C_{tot} at a fixed concentration of $MgCl_2$ (Appendix C). The effect of added salt on η_0 for $C_{tot} = 14$ wt% becomes insignificant. Similar observations are reported in the literature for the mixed solutions of CAPB and sulfonated methyl esters [7] and for CAPB and sodium dodecylbenzenesulfonate [58]. Nevertheless, the transition from wormlike to branched micelles takes place at one and the same $C_{salt} \approx 30$ mM $MgCl_2$ for all studied surfactant concentrations from 5 wt% to 14 wt% (Fig. 4a).

In the case of crystal formation, the salting-out effect leads to low viscous solutions with $\eta_{0.01}$ about 1–2 Pa.s. The shear thinning at high shear rates takes place for all studied salt and surfactant concentrations. For $C_{salt} < 150$ mM, the Newtonian behavior is not reached even for $\dot{\gamma} = 100\ s^{-1}$ and η_{100} varies from 0.1 to 1 Pa.s (Fig. 4b). For $C_{salt} > 150$ mM, the shear thinning of micellar solutions is well pronounced and the fluids obey Newtonian behavior at high shear rates with well-defined values of η_∞.

Fig. 4c summarizes the dependencies of the zero-shear viscosity on the surfactant concentration for $C_{salt} = 12$, 20, and 25 mM and wormlike micellar solutions. One sees that the power law indexes decrease with the rise of C_{salt}: 10.8 ± 0.5 for 12 mM $MgCl_2$; 7.0 ± 0.8 for 20 mM $MgCl_2$; 5.7 ± 0.9 for 25 mM $MgCl_2$. In all illustrated cases, the calculated indexes are considerably greater than the range from 3 to 3.5 reported in the literature [10,24]. The maximum measured values of η_0 (at the peaks of the viscosity flow curves, Fig. 4a) have close values and do not follow the power law dependence. In the case of branched micelles, η_0-vs.-C_{tot} curve at $C_{salt} = 60$ mM follows the power law with an index equal to 4.6 ± 0.3, which is again greater than the theoretical one from 1 to 2.5 [10,24]. These observations show that the dependence of the micelle growth and the zero-shear viscosity on the total concentration of

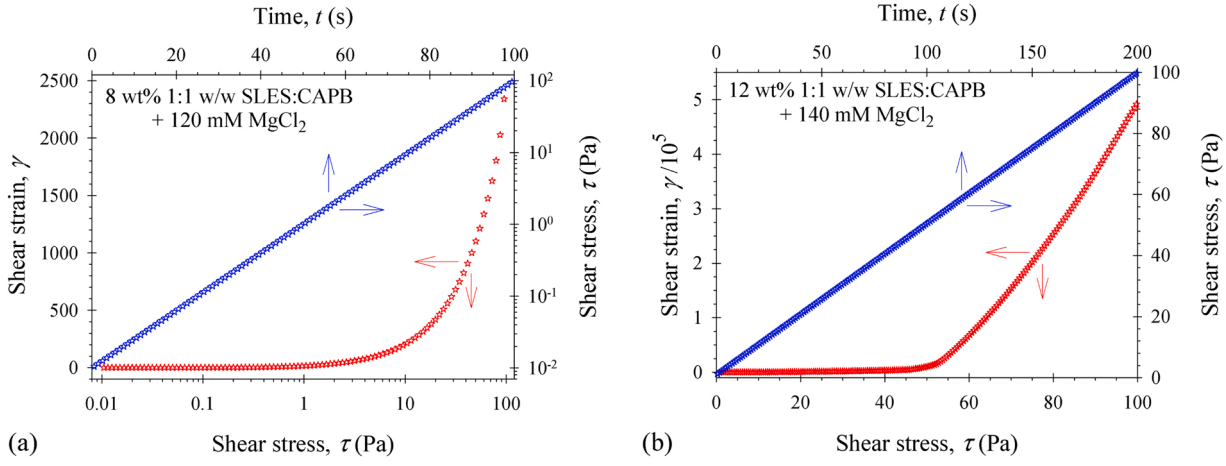

Fig. 2. Shear strain, γ, vs. shear stress, τ, measured for BMPs: (a) isolated from 8 wt% 1:1 w/w SLES:CAPB + 120 mM $MgCl_2$ and an exponential increase of the shear stress with time (PP 40); (b) isolated from 12 wt% 1:1 w/w SLES:CAPB + 140 mM $MgCl_2$ and a linear increase of τ with t (CP 2/60).

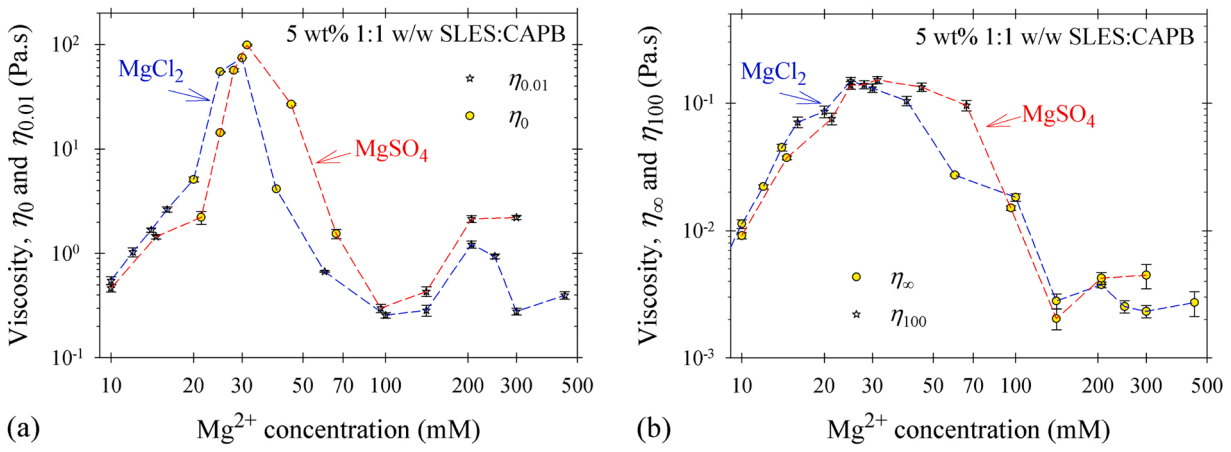

Fig. 3. Dependence of the apparent viscosity of 5 wt% 1:1 w/w SLES:CAPB micellar solution on the concentration of added salt: (a) zero-shear viscosity η_0 and $\eta_{0.01}$; (b) Newtonian viscosity η_∞ and η_{100}.

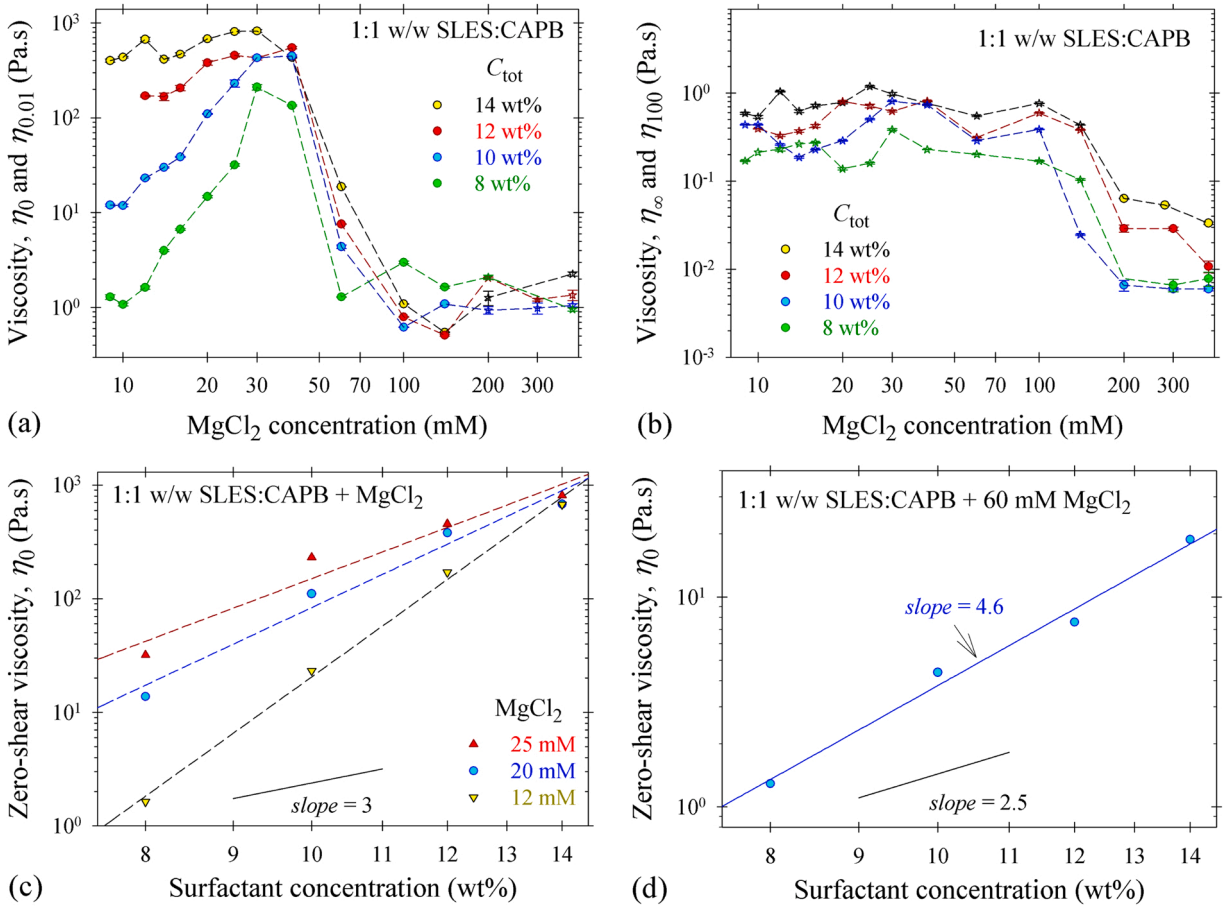

Fig. 4. Dependence of the apparent viscosity of 1:1 w/w SLES:CAPB micellar solution on the concentration of added salt for different C_{tot}: (a) zero-shear viscosity and $\eta_{0.01}$; (b) viscosities at high shear rates η_∞ and η_{100}; (c) zero-shear viscosity vs. C_{tot} for wormlike micellar solutions; (d) η_0 vs. C_{tot} for solutions with branched micelles, C_{salt} = 60 mM.

mixed surfactant solutions is more complex than expected and further theoretical studies are needed.

4. Rheology of solutions with wormlike and branched micelles in an oscillatory regime

The rheological experiments in oscillatory regimes give the possibility to distinguish the solutions with wormlike and branched micelles. For that purpose, it is important to determine $G'(\omega)$ and $G''(\omega)$ in a linear regime (Fig. 1d and Appendix D). In all reported experiments bellow, the shear strain amplitude of oscillations, γ_a, was equal to 0.02 in order to ensure the linear response of the systems.

For a viscoelastic continuum with constant elasticity G_0 and viscosity η_0, the storage and loss moduli obey the Maxwell rheological model:

$$G' = G_0\frac{(\tau_R\omega)^2}{1+(\tau_R\omega)^2}\ ,\ G'' = G_0\frac{\tau_R\omega}{1+(\tau_R\omega)^2} \quad (1)$$

where the relaxation time is $\tau_R = \eta_0/G_0$. The range of frequencies, for which G_0 and η_0 have constant values, is checked using the Cole-Cole plot:

$$\left(\frac{2G'}{G_0}-1\right)^2+\left(\frac{2G''}{G_0}\right)^2 = 1 \quad (2)$$

i.e. G' and G'' obey an equation of a circle of radius $G_0/2$ (Fig. 5a).

Fig. 5a shows the Cole-Cole plot of the experimental data for the storage and loss moduli measured for wormlike micellar solutions in the presence of 20 mM $MgCl_2$ at three surfactant concentrations: 10, 12, and 14 wt%. The best theoretical values of elasticity G_0, relaxation time τ_R, and viscosity η_0, calculated from Eq. (1) in the range of its validity, are summarized in Table 1.

The Cates theory for living polymers [18–21] is widely used in the literature to characterize the deviations from the Cole-Cole plot in the case of semi-diluted wormlike micellar solutions [6,7,59]. The reptation-reaction model accounts for two relaxation processes: the reaction of micelle reversible breakage and recombination is characterized by relaxation time τ_{br}; the curvilinear diffusion of a wormlike micelle between the neighboring micelles is accounted for by relaxation time τ_{rep}. For small values of the ratio $\zeta \equiv \tau_{br}/\tau_{rep}$ (typically observed at low oscillation frequencies), the stress relaxation is exponential – the storage and loss moduli obey the Maxwell equations, Eq. (1). The theoretical dependence of $\overline{\zeta} \equiv \tau_{br}/\tau_R$ can be obtained by numerical solutions of the respective statistical equations [21]. It is shown in the literature [7,59] that $\overline{\zeta}^2 = 5\zeta$ and $\tau_R = 0.447(\tau_{br}\tau_{rep})^{1/2}$ for $\zeta \le 10$. Finally, for flexible micelles in a semi-diluted regime, the mesh size (the correlation length) of the transient micellar network, ξ, is estimated from the following relationship: $\xi \approx (k_BT/G_0)^{1/3}$, where k_B is the Boltzmann constant and T is the absolute temperature [18,21]. The obtained rheological parameters from the best fit of the experimental data in Fig. 5a according to the Cates model are given in Table 1.

The following conclusions can be drawn from the obtained results reported in Table 1. First, the experimental values of the zero-shear viscosity, η_0, measured in the steady-shear regime illustrated in Fig. 4a are close to the theoretical values of $G_0\tau_R$ calculated from the oscillatory experiments (Fig. 5a) – the Cox-Merz rule [60] is fulfilled. The independent rheological measurements lead to close results for η_0, which proves the applicability of the Cates model. The reptation time, τ_{rep}, is proportional to the cube of the mean length of the wormlike micelles, so that the increase of τ_{rep} with C_{tot} (the increase of the mean length of micelles) is reasonable. The increase of the elasticity, G_0, is due to the decrease of the mesh size of micellar network, ξ, with the increase of surfactant concentration. The increase of τ_{br} and the decrease of G_0 (see Table 1) suggest that the micelles become less flexible and with a greater persistence length with the decrease of the total surfactant concentration.

The ratio ζ for $C_{tot} = 10$ wt% is greater than 1 and the further decrease of the surfactant concentration ($C_{tot} = 8$ wt% and $C_{salt} = 20$ mM) increases ζ so much that the deviations of G' and G'' from the Cole-Cole plot are measured for very low frequencies (see Appendix D) even for intermediate values of the zero-shear viscosity, $\eta_0 = 14.8$ Pa.s (Fig. 4a). In this case the augmented version of the Maxwell model [7] relates the mean characteristic frequency of the system, $<\nu_{ch}>$, with the relaxation time, τ_R, at low values of ω, and a coefficient $1/\tau_F$ to scale the frequency dependence:

$$<\nu_{ch}> \equiv \frac{G''}{G'}\omega = \frac{1}{\tau_R}+\frac{1}{\tau_F}\left(\frac{\omega}{\omega_0}\right)^m \quad (3)$$

where $\omega_0 = 1$ rad/s. The power law index, m, characterizes the thixotropy of the solutions. The experimental data for $<\nu_{ch}>$ in the case of wormlike micellar solution with $C_{tot} = 8$ wt% and $C_{salt} = 20$ mM are excellently described with Eq. (3), see Appendix D. The obtained parameters are: $\tau_R = 1.03 \pm 0.06$ s; $\tau_F = 1.60 \pm 0.06$ s; $m = 0.93 \pm 0.01$. One sees that the relaxation time is two times lower than that for the solution with $C_{tot} = 10$ wt% (c.f. Table 1).

In this version of the Maxwell model, the mean elasticity, $<G>$, and viscosity, $<\eta>$, are calculated from the following expressions [7]:

$$<G> = \frac{(G')^2+(m+1)(G'')^2}{G'} - m\frac{G''}{\tau_R\omega}\ ,\ <\eta> = \frac{<G>}{<\nu_{ch}>} \quad (4)$$

Note that $<G> \to G_0$ and $<\eta> \to \eta_0$ at the limit of very low frequencies $\omega \to 0$. Fig. 5b shows the dependence of the mean shear elasticity and shear viscosity on the frequency of oscillations. With the increase of ω, this micellar solution becomes more elastic and less viscous. The limit value of the viscosity at low frequencies is 15.8 Pa.s, which is close to the zero-shear viscosity of 14.8 Pa.s shown in Fig. 4a. The corresponding elasticity, $G_0 = 15.3$ Pa, is lower than that for $C_{tot} = 10$ wt% (c.f. Table 1) because of the lower surfactant concentration and a wider mesh size of the micellar network.

The surfactant solutions contain branched micelles on the right of the maximum of the salt curves (Fig. 4a) in the presence of 60 mM $MgCl_2$. Fig. 6a shows the Cole-Cole plots for $C_{tot} = 10$, 12, and 14 wt%. It is well seen that the Maxwell equations, Eq. (1), describe well the viscoelastic properties of these solutions up to high frequencies of oscillations (see Fig. D4). However, the obtained values of the elasticity, G_0, and the relaxation time, τ_R, are considerably different than those for wormlike micellar solutions at the same surfactant concentrations (cf. Tables 1 and 2). The relaxation times are more than 45 times shorter for branched micelles compared to those for wormlike micelles. For branched

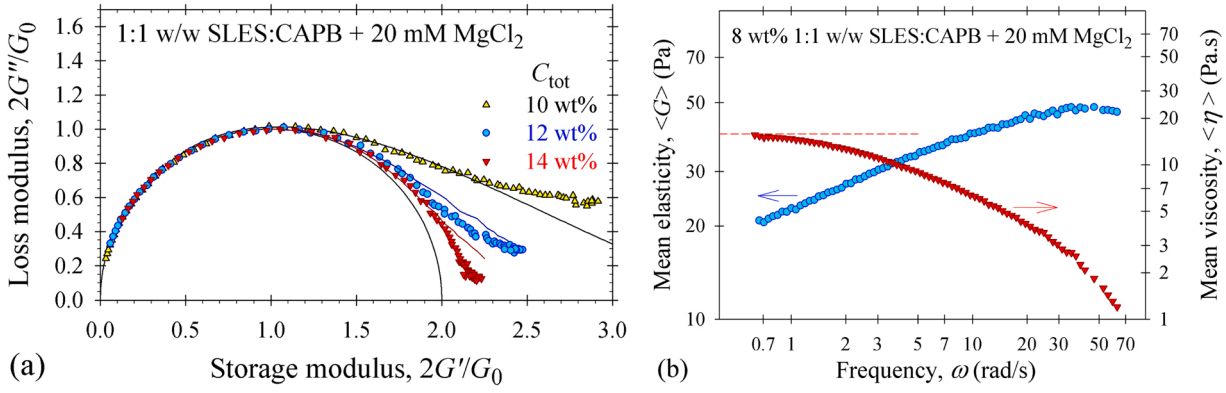

Fig. 5. Wormlike micellar solutions in the presence of 20 mM $MgCl_2$: (a) Cole-Cole plot for $C_{tot} = 10$, 12, and 14 wt%; (b) mean elasticity, $<G>$, and viscosity, $<\eta>$, for $C_{tot} = 8$ wt%.

Table 1
Rheological parameters of the wormlike micellar solutions in the presence of 20 mM $MgCl_2$ at three total surfactant concentrations.

C_{tot} (wt%)	η_0 (Pa·s)	G_0 (Pa)	τ_R (s)	$G_0\tau_R$ (Pa·s)	ξ (nm)	$\bar{\zeta}$ (–)	ζ (–)	τ_{br} (s)	τ_{rep} (s)
10	110	61.5	2.02	124	40.6	2.38	1.13	4.81	4.25
12	380	135	2.77	374	31.2	1.23	0.303	3.41	11.3
14	678	200	3.44	688	27.4	0.70	0.098	2.41	24.6

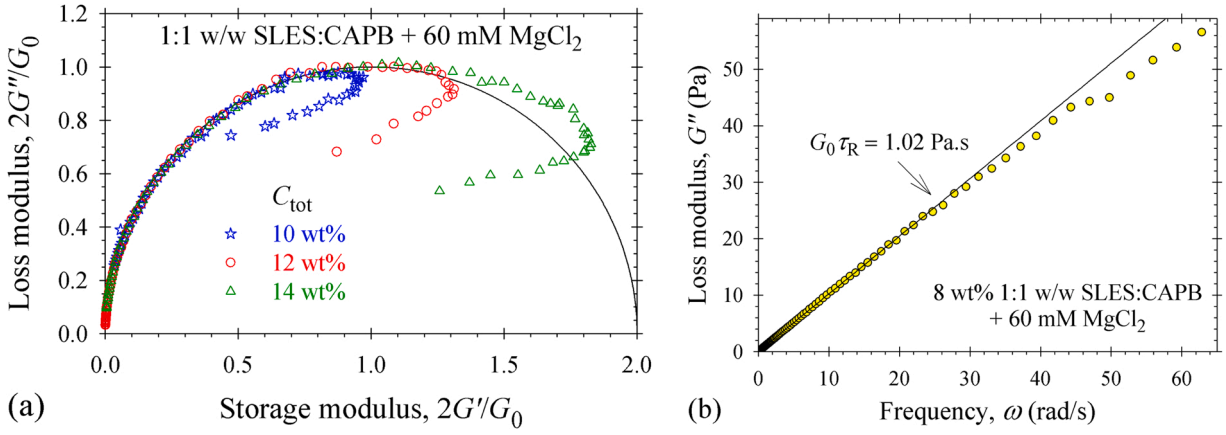

Fig. 6. Branched micellar solutions in the presence of 60 mM $MgCl_2$: (a) Cole-Cole plot for C_{tot} = 10, 12, and 14 wt%; (b) loss modulus, G'', vs. frequency, ω, for C_{tot} = 8 wt%.

Table 2
Rheological parameters of the branched micellar solutions in the presence of 60 mM $MgCl_2$ at four total surfactant concentrations.

C_{tot} (wt%)	η_0 (Pa·s)	G_0 (Pa)	τ_R (s)	$G_0\tau_R$ (Pa·s)
8	1.29	–	–	1.02
10	4.38	180	0.0193	3.47
12	7.59	232	0.0329	7.63
14	18.8	228	0.0768	17.5

micelles, the elasticities, G_0, are higher because of the more tangled structure of the branched micelles than that of the wormlike micelles at a given surfactant concentration. As a result, the viscosities, $G_0\tau_R$, for C_{salt} = 60 mM are lower than those for added 20 mM $MgCl_2$, cf. Figs. 4c and 4d and Tables 1 and 2. It is remarkable that the values of the product $G_0\tau_R$ determined from the data in the oscillatory regime in the case of branched micelles are again in good agreement with the values of η_0 independently obtained from the respective flow curves (Table 2). This coincidence is an argument in favor of the self-consistence of the Maxwell model.

The deviations from the Cole-Cole plot illustrated in Fig. 6a have different shapes than those in Fig. 5a. From our knowledge, there is no a theoretical model reported in the literature to describe this type of deviations in the case of branched micelles. The oscillatory experiments (cf. Figs. 5a and 6a) can be used to distinguish wormlike and branched micellar structures for solutions with close values of the zero-shear viscosities.

In the case of 8 wt% surfactant concentration and C_{salt} = 60 mM, the measured storage moduli are much lower than the loss moduli (Appendix D) for all experimental frequencies of oscillations. Thus, the asymptotic form of Eq. (1) leads to the simple relationship: $G'' \approx (G_0\tau_R)\omega$. Fig. 6b shows that this simple asymptotic equation is valid for $\omega < 30$ rad/s, from where the slope of the linear plot gives $G_0\tau_R$ = 1.02 Pa.s (Table 2). Again, the zero-shear viscosity is close to $G_0\tau_R$ and the branched micellar solution obeys the Maxwell law for $\omega < 30$ rad/s.

5. Rheological properties of bicontinuous micellar phases

In this section we present the rheological characteristics of the BMPs, isolated from the separated sediments of the studied micellar solutions (Appendix A). The concentrations, C_{tot} and C_{salt}, used below correspond to those of the micellar solution, from which the BMP was isolated.

Fig. 7a shows the dependence of the apparent viscosity, η, on the shear rate, $\dot{\gamma}$, obtained in the steady-shear regime for five bicontinuous micellar phases isolated from 1 wt% surfactant solutions containing different $MgCl_2$ concentrations. One sees that the zero-shear viscosity of these phases is independent on $MgCl_2$ concentration. The same conclusion for C_{tot} = 5 wt% is reported in Ref. [52]. The respective flow curves for 3, 8, 10, and 12 wt% are summarized in Fig. E1. The zero-shear viscosity for all studied five total surfactant concentrations, 3 wt% $\leq C_{tot} \leq$ 12 wt%, and different added $MgCl_2$ concentrations is constant and equal to 0.66 ± 0.01 Pa.s. Only at the lowest total surfactant concentration (C_{tot} = 1 wt%), lower value of η_0 = 0.40 ± 0.01 Pa.s is measured (Fig. 7a).

Plots in Fig. 7a and E1 show that there is a transitional shear rate, $\dot{\gamma}_{tr}$, after which the apparent viscosity decreases with the shear rate because of the pseudoplastic behavior of the BMPs. For the precise determination of $\dot{\gamma}_{tr}$, we plot the shear stress, τ, as a function of the shear rate, $\dot{\gamma}$ (Fig. 7b). In the region with quasi-Newtonian behavior and zero-shear viscosity, $\tau = \eta_0\dot{\gamma}$, the slope defines the most probable value of η_0. The well pronounced deviation of the experimental τ – vs. – $\dot{\gamma}$ dependence from the straight line determines $\dot{\gamma}_{tr}$ (Fig. 7b).

It was observed in Ref. [52], that the transitional shear rate for C_{tot} = 5 wt% is a linear function on the added $MgCl_2$ concentration. Fig. 7c shows that analogous linear dependences are measured also for other three total surfactant concentrations, C_{tot} = 1, 3, and 8 wt%. The intersections of the straight lines with horizontal axis define the threshold concentration, C_{sep}, of $MgCl_2$ needed to observe a phase separation. For $C_{salt} < C_{sep}$, we do not observe the separation of droplets from the multiconnected micellar phase and their sedimentation at the bottom of the vessel.

For surfactant concentrations above 8 wt%, the regions of $MgCl_2$ concentrations for the sedimentation of the BMP become narrower with

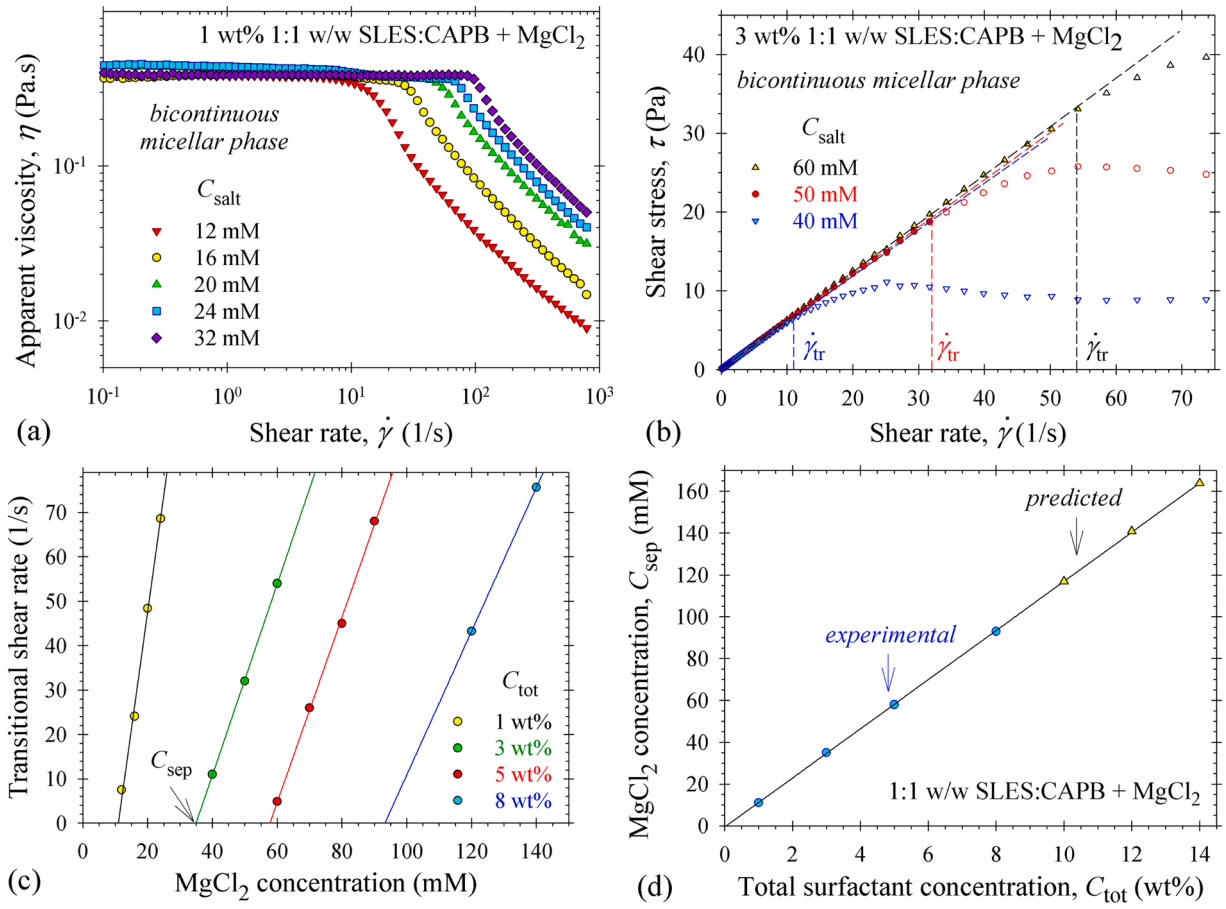

Fig. 7. Rheological properties of BMPs in a steady-shear regime. (a) Apparent viscosity vs. shear rate for C_{tot} = 1 wt% and different C_{salt}. (b) Shear stress vs. shear rate – determination of the zero-shear viscosity, η_0, from the slope at $\dot{\gamma}\rightarrow 0$ and determination of the transitional shear rate, $\dot{\gamma}_{tr}$, that characterizes the transition from quasi-Newtonian to shear-thinning behavior. (c) Plot of $\dot{\gamma}_{tr}$ vs. C_{salt}; C_{sep} is the first salt concentration, at which a phase separation of the BMP appears. (d) Dependence of C_{sep} on the total surfactant concentration.

the increase of C_{tot} (Appendixes A and D) – there are not enough points to construct the $\dot{\gamma}_{tr} - \text{vs.} - C_{salt}$ line and to calculate C_{sep}. Fig. 7d shows the obtained experimental dependence of C_{sep} on the total surfactant concentration, C_{tot}. The following simple empirical rule is found: $C_{sep} = -0.58 + 11.75C_{tot}$, where C_{sep} is measured in mM and C_{tot} in wt%. The predictions of this rule for larger surfactant concentrations (C_{sep} = 117 mM for 10 wt%; C_{sep} = 140 mM for 12 wt%; C_{sep} = 164 mM for 14 wt%) agree well with the results reported in Appendix A.

The systematic rheological experiments with the BMPs in the stress-ramp regime ($\dot{\tau} = 0$) suggest that these complex fluids have yield stresses. Thus, we should include the Bingham element with yield stress τ_0 in the Maxwell scheme (Fig. 8). Fig. 9 summarizes experimental data for the apparent viscosity of the BMP isolated from 12 wt% surfactant solution in the presence of 140 mM $MgCl_2$ (element CP 2/60). The illustrated experimental data are obtained as follows: in a stress-ramp regime with an exponential increase of τ (curve A); η–vs.–$\dot{\gamma}$ (flow curve C); in a stress-ramp regime with a linear increase of τ (curve B).

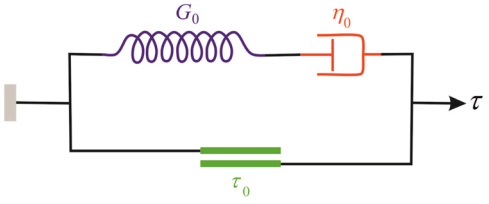

Fig. 8. Rheological model of the BMP: elastic element with elasticity G_0; viscous element with viscosity η_0; Bingham element with yield stress τ_0.

Similar shapes for η–vs.–$\dot{\gamma}$ are observed for C_{salt} = 160 and 180 mM (see Appendix E). One sees that the combination of the three rheological regimes gives the possibility to cover more than seven orders of magnitude range of the shear-rate variations: from 2×10^{-4} to 7×10^{3} s^{-1}. It is remarkable that the different regimes match excellently: A tends to C for shear rate 0.1 s^{-1}; C tends to B for shear rate 100 s^{-1}. As it should be, a pronounced shear thinning is measured for high enough shear rates. For very low shear rates, the apparent viscosity decreases from 45 Pa.s to 0.66 Pa.s (see curve A in Fig. 9a). In the case of $\dot{\tau} = 0$, the elasticity, G_0, does not influence the rheological response and $\tau = \tau_0 + \eta_0\dot{\gamma}$ (see Fig. 8).

Thus, for all measurements of type A, the apparent viscosity is a linear function of the inverse shear rate:

$$\eta = \eta_0 + \frac{\tau_0}{\dot{\gamma}} \left(\text{stress} - \text{rampregime}\right) \quad (5)$$

Fig. 9b presents all experimental data for the apparent viscosities of the BMPs isolated from 12 wt% surfactant solutions with different amount of added $MgCl_2$ measured in the stress-ramp regime (type A). From the slope of η-vs.-$\dot{\gamma}^{-1}$ curve, we calculated the yield stress: $\tau_0 = 11.8 \pm 0.2$ mPa. Although the low value of τ_0, it is well defined as witnessed by the good regression coefficient of 0.9998.

To prove the validity of the proposed combined model (Fig. 8), we performed stress relaxation experiments using the following protocol: the shear strain increases for 20 s with a constant $\dot{\gamma}$ to 30, 50, 70, and 90; subsequently the relaxation of the shear stress is measured for 40 s at a fixed shear strain (Fig. 9c). Initially, the shear stress suddenly increases

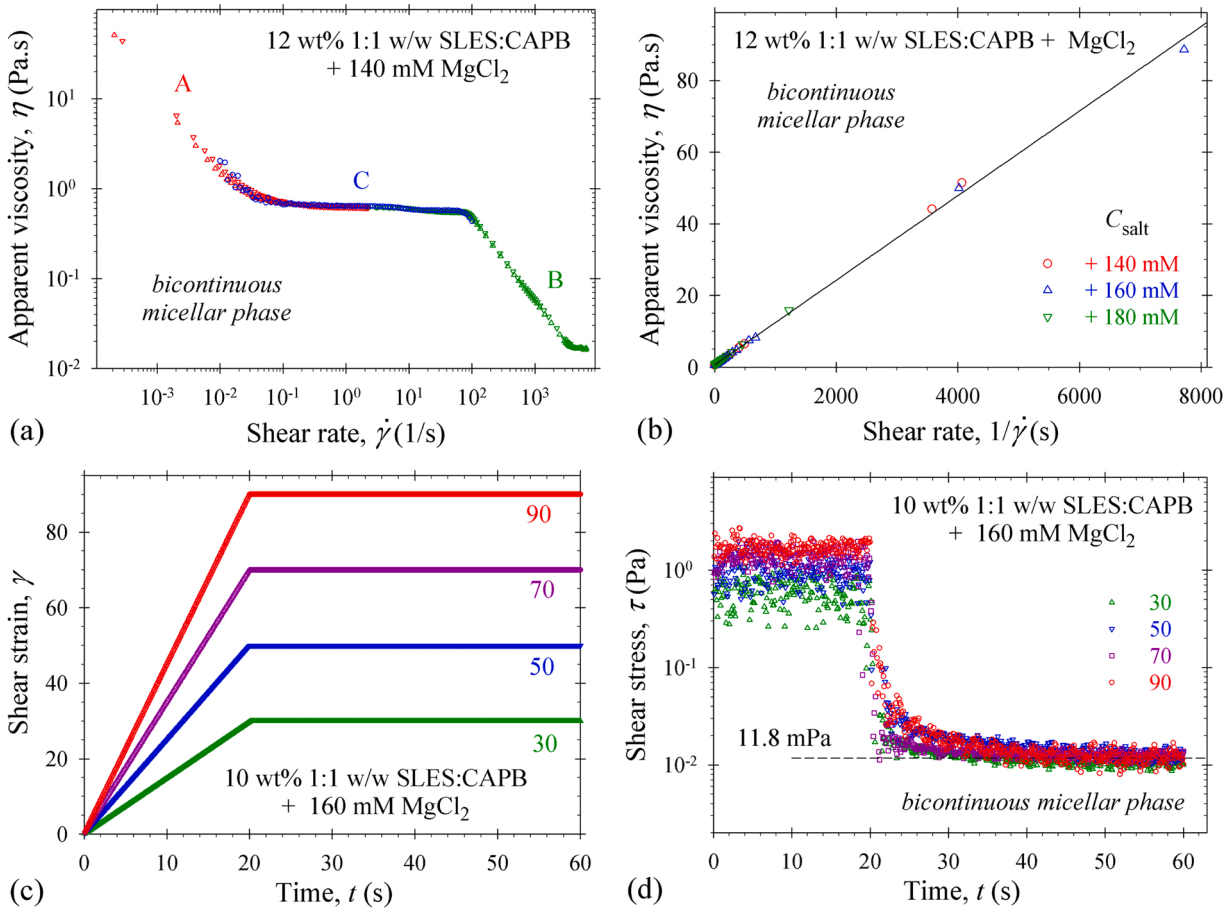

Fig. 9. Rheological behavior of the BMPs studied using different regimes. Isolated from 12 wt% surfactant solutions with different C_{salt}: (a) η vs. shear rate in the stress-ramp regime (A and B) and in the steady-shear regime (C); (b) η vs. $\dot{\gamma}^{-1}$ from the stress-ramp regime (A). Isolated from 10 wt% surfactant solutions in the presence of 160 mM $MgCl_2$: (c) shear strain increases with a constant $\dot{\gamma}$ for 20 s and subsequently it is kept constant; (d) measured resulting shear stress with time corresponding to the respective shear deformations.

because of the short relaxation times, η_0/G_0. At different constant shear strains, the shear stresses relax to one and the same value equal to the yield stress of 11.8 mPa. Note that the yield stress of the BMPs does not depend on C_{tot} and C_{salt} as it was observed for the zero-shear viscosity.

The experimental yield stress of complex fluids depends on the thickness of the shearing layers. To illustrate the specificity of the yield stress, we performed experiments in the stress-ramp regime (type A) using elements PP 40 and Vane of the rheometer (Fig. 10). The solid lines plotted in Fig. 10 show the best fit with the simple model, Eq. (5).

The obtained yield stress in the case of working element PP 40 is

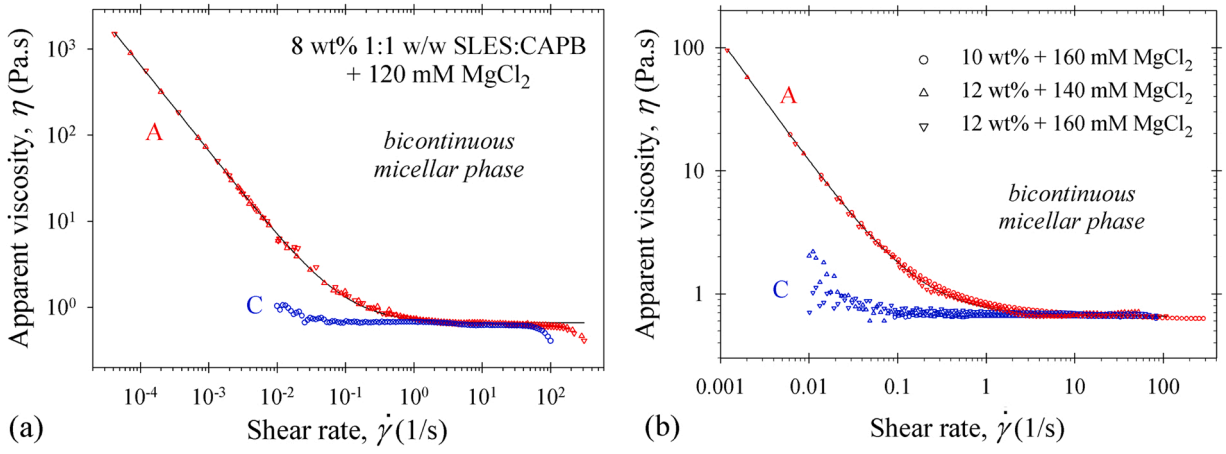

Fig. 10. Flow curves for BMPs measured in the steady-shear regime (C) using element CP 2/60. The apparent viscosity vs. shear rate obtained in the stress-ramp regime (A) for BMPs is measured with different working elements of the rheometer: (a) BMP isolated from 8 wt% 1:1 SLES:CAPB + 120 mM $MgCl_2$ and element PP 40; (b) BMP isolated from 10 wt% surfactant solutions in the presence of 160 mM $MgCl_2$ and from C_{tot} = 12 wt% and C_{salt} = 140 and 160 mM solutions and element Vane.

$\tau_0 = 65.0 \pm 0.5$ mPa (Fig. 10a) and that from measurements with element Vane is $\tau_0 = 115 \pm 1$ mPa (Fig. 10b). Note that the apparent viscosities measured at high shear rates using different geometries and rheological protocols coincide in the frame of experimental errors (see Figs. 9a and 10). In the case of solid materials, one should destroy the structure of the whole material to overcome the yield stress. In our case, the thickness of the solution layer is the smallest for element CP 2/60, which has smooth surfaces and we determined the lowest value of $\tau_0 = 11.8$ mPa. The thickness of the solution layer is larger in the case of working element PP 40 and the determined yield stress increases to $\tau_0 = 65.0$ mPa. Finally, the element Vane has a complex geometry (see Appendix B), in which the respective thickness of the shearing zone is the greatest and we measured the largest $\tau_0 = 115$ mPa.

Fig. 11 shows the dependence of the determined yield stresses, τ_0, of the BMP on the ratio between the shearing volume of the solution and the area of the shearing surfaces of the used working elements of the rheometer. The shearing force is equal to the yield stress multiplied by the area of the shearing surfaces, so that the shearing force increases with the rise of the volume of BMP. This result suggests that the bicontinuous micellar phase is a homogeneous structure and to overcome the yield stress, one needs to apply a shearing force proportional to the whole shearing volume of the BMP for thin enough shearing layers.

6. Conclusions

The phase separation of saturated micellar network as a result of interconnection of branched micelles has been reported in the literature [30,52]. The isolated BMPs have a nanoemulsification capacity in the presence of small organic molecules (limonene, linalool, citronellol, etc.). For example, the amount of solubilized limonene is two times larger than the total amount of surfactants [52]. The nanoemulsification of oily substances by BMP can find applications for the low energy cost production of nanoemulsions with their numerous applications [61–63]. In the present article, an advanced rheological study of the mixed micellar surfactant solutions is applied to characterize and distinguish different micellar structures – from wormlike and branched micelles to bicontinuous micellar phases.

The phase behavior of concentrated base solutions (1:1 wt ratio of anionic laurylethersulfate with one ethylene oxide group, SLES, and zwitterionic cocamidopropyl betaine, CAPB) at different surfactant concentrations (1 wt% $\leq C_{tot} \leq$ 14 wt%) in the presence of divalent counterions (Mg^{2+}) shows five regions with the rise of concentration, C_{salt}, of added salt ($MgCl_2$ and $MgSO_4$): spherocylindrical micelles (for lower surfactant concentrations); wormlike micelles; branched micelles;

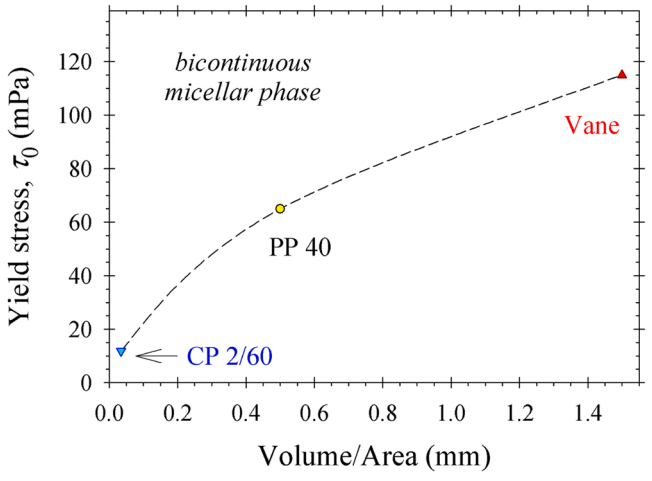

Fig. 11. Dependence of the yield stress, τ_0, of the BMP on the ratio between the shearing volume and the area of the shearing surfaces of the used working elements of the rheometer.

formation of droplets of saturated micellar network; crystal formation because of the salting out of surfactants. The significantly different rheological behavior of solutions containing these micellar structures becomes a powerful tool to relate the rheology and microstructures of complex fluids. For low shear rates, all studied systems obey the Maxwell type model (see Fig. 8) with constant elasticities and viscosities. The different types of micellar solutions have different physical explanation of the decrease of shear viscosity in the shear thinning regime for high shear rates. For wormlike micellar solutions, the Cates theory for living polymers [18–21] is widely used in the literature. For branched micellar solutions, the movement of branches along a micelle contour has been proposed as a mechanism of stress relaxation that leads to a reduction in the structural relaxation time and thus, the zero-shear viscosity [64]. In the case of BMP, the quasi-Newtonian behavior takes place up to very high shear rates.

The studied wormlike micellar solutions are characterized with a well pronounced relatively high zero-shear viscosity, η_0, and elasticity, G_0 (Figs. 3 and 4). The oscillatory experiments are described excellently with the Cates theory for living polymers [18–21] and the augmented version of the Maxwell model [7], which provide independent information on the relaxation processes (reptation, breakage and characteristic frequency) and the characteristic mesh size of the micellar network. In all cases, the validity of the Cox-Merz rule [60] proves the self-consistence of the applied models. The effect of added divalent counterion concentration, C_{salt}, leads to a pronounced change of the power law index of the η_0-vs.-C_{tot} dependence, which varies from 5.7 (at 25 mM $MgCl_2$) to 10.8 (at 12 mM $MgCl_2$). The branched micellar solutions also exhibit quasi-Newtonian behavior at low shear rates with well-defined η_0. They follow the Maxwell rheological law up to high frequencies of oscillations (Fig. 6) with orders of magnitude lower relaxation time. Even at comparable values of the zero-shear viscosities of wormlike and branched micellar solutions, the Cole-Cole plots of the storage and loss moduli are considerably different (cf. Figs. 5a and 6a) and can be used to distinguish these micellar structures.

At high enough divalent counterion concentration, the sedimented drops of saturated micellar network coalesce and form a separate bicontinuous micellar phase (BMP). The specific rheological properties of the isolated BPM are systematically described in Section 5. First, the BMPs have a unique viscosity of about 0.66 Pa.s, which is independent on the surfactant and salt concentration of micellar solutions, from which these phases were separated. The analysis of the transition shear rates from quasi-Newtonian to shear-thinning regime allow us to define a simple empirical law for the threshold concentration of $MgCl_2$, C_{sep}, needed to observe BMP separation (Fig. 7). The BMP has high elasticities, low relaxation times, and well-defined yield stresses. Using different working elements of the rheometer and appropriate rheological regimes gave the possibility to cover the wide range of shear rates, from 2×10^{-4} to 7×10^{3} s^{-1} (Fig. 9) and to measure the yield stress of the BMP. The yield stress, τ_0, also has a unique value independent on the surfactant and salt concentration of base micellar solutions. The dependence of the determined BMP yield stresses on the ratio between the shearing volume of the solution and the area of the shearing surfaces shows that the bicontinuous micellar phase is a homogeneous compact structure, which is fluidized at a shearing force proportional to the whole shearing volume for thin enough shearing layers (Fig. 11).

Further development of the present study could include: (i) the investigation of the possibilities to separate BMPs from different surfactant mixtures in the presence of multivalent counterions; (ii) systematic characterization of the BMPs important for the production of macroscopic amounts of such phases with preliminary defined rheological properties for a given practical application.

CRediT authorship contribution statement

T.N. Stancheva: Data curation. **M.T. Georgiev**: Conceptualization, Investigation, Methodology. **G.M. Radulova**: Investigation, Data

curation, Methodology. **K.D. Danov**: Conceptualization, Software, Formal analysis, Supervision, Writing – original draft. **K.G. Marinova**: Conceptualization, Methodology.

Declaration of Competing Interest

The authors declare the following financial interests/personal relationships which may be considered as potential competing interests: K. D. Danov reports financial support was provided by Republic of Bulgaria Ministry of Education and Science. K.G. Marinova reports financial support was provided by Republic of Bulgaria Ministry of Education and Science. M.T. Georgiev reports financial support was provided by Republic of Bulgaria Ministry of Education and Science. G.M. Radulova reports financial support was provided by Republic of Bulgaria Ministry of Education and Science. T.N. Stancheva reports financial support was provided by Republic of Bulgaria Ministry of Education and Science.

Data availability

Data will be made available on request.

Acknowledgements

The authors gratefully acknowledge the support from the Natural Science Fund of Bulgaria, Grant No. КП-06-ПН 49/5, and from the Operational Programme “Science and Education for Smart Growth,” Bulgaria, project No. BG05M2OP001-1.002-0023.

Declaration of Competing Interest

The authors declare that they have no known competing financial interests or personal relationships that could have appeared to influence the work reported in this paper.

Appendix A. Supporting information

Supplementary data associated with this article can be found in the online version at doi:10.1016/j.colsurfa.2022.129927.

References

[1] H. Hoffmann, A. Rauscher, M. Gradzielski, S.F. Schulz, Influence of ionic surfactants on the viscoelastic properties of zwitterionic surfactant solutions, Langmuir 8 (1992) 2140–2146, https://doi.org/10.1021/la00045a013.
[2] S. Hofmann, H. Hoffmann, Shear-induced micellar structures in ternary surfactant mixtures: the influence of the structure of the micellar interface, J. Phys. Chem. B 102 (1998) 5614–5624, https://doi.org/10.1021/jp980339w.
[3] D. Danino, A. Bernheim-Groswasser, Y. Talmon, Digital cryogenic transmission electron microscopy: an advanced tool for direct imaging of complex fluids, Colloids Surf. A 183 (2001) 113–122, https://doi.org/10.1016/S0927-7757(01)00543-X.
[4] N. Dan, K. Shimoni, V. Pata, D. Danino, Effect of mixing on the morphology of cylindrical micelles, Langmuir 22 (2006) 9860–9865, https://doi.org/10.1021/la061254m.
[5] D.P. Acharya, H. Kunieda, Wormlike micelles in mixed surfactant solutions, Adv. Colloid Interface Sci. 123–126 (2006) 401–413, https://doi.org/10.1016/j.cis.2006.05.024.
[6] S. Różańska, Rheology of wormlike micelles in mixed solutions of cocoamidopropyl betaine and sodium dodecylbenzenesulfonate, Colloids Surf. A 482 (2015) 394–402, https://doi.org/10.1016/j.colsurfa.2015.06.045.
[7] V.I. Yavrukova, G.M. Radulova, K.D. Danov, P.A. Kralchevsky, H. Xu, Y.W. Ung, J. T. Petkov, Rheology of mixed solutions of sulfonated methyl esters and betaine in relation to the growth of giant micelles and shampoo applications, Adv. Colloid Interface Sci. 275 (2020), 102062, https://doi.org/10.1016/j.cis.2019.102062.
[8] G. Tyagi, D. Seddon, S. Khodaparast, W.N. Sharratt, E.S.J. Robles, J.T. Gabral, Tensiometry and FTIR study of the synergy in mixed SDS:DDAO surfactant solutions at varying pH, Colloids Surf. A 618 (2021), 126414, https://doi.org/10.1016/j.colsurfa.2021.126414.
[9] V. Hartmann, R. Cressely, Linear and nonlinear rheology of a wormlike micellar system in presence of sodium tosylate, Rheol. Acta 37 (1998) 115–121, https://doi.org/10.1007/s003970050097.
[10] A. Parker, W. Fieber, Viscoelasticity of anionic wormlike micelles: effects of ionic strength and small hydrophobic molecules, Soft Matter 9 (2013) 1203–1213, https://doi.org/10.1039/C2SM27078A.
[11] S. Amin, S. Blake, R.C. Kennel, E.N. Lewis, Revealing new structural insights from surfactant micelles through DLS, microrheology and Raman spectroscopy, Materials 8 (2015) 3754–3766, https://doi.org/10.3390/ma8063754.
[12] H. Tang, W. Zou, P.H. Koenig, S.D. McConaughy, M.R. Weaver, D.M. Eike, M. J. Schmidt, R.G. Larson, Multiscale modeling of the effects of salt and perfume raw materials on the rheological properties of commercial threadlike micellar solutions, J. Phys. Chem. B 121 (2017) 2468–2485, https://doi.org/10.1021/acs.jpcb.7b00257.
[13] E. Cappelaere, R. Cressely, Rheological behavior of an elongated micellar solution at low and high salt concentrations, Colloid Polym. Sci. 276 (1998) 1050–1056, https://doi.org/10.1007/s003960050346.
[14] E. Cappelaere, R. Cressely, Influence of $NaClO_3$ on the rheological behavior of a micellar solution of CPCl, Rheol. Acta 39 (2000) 346–353, https://doi.org/10.1007/s003970000095.
[15] H.A. Sheraga, Non-Newtonian viscosity of solutions of ellipsoidal particles, J. Chem. Phys. 23 (1955) 1526–1532, https://doi.org/10.1063/1.1742341.
[16] T.M. Kwon, M.S. Jhon, H.J. Choi, Viscosity of magnetic particle suspension, J. Mol. Liq. 75 (1998) 115–126, https://doi.org/10.1016/S0167-7322(98)82000-X.
[17] P.G. de Gennes, Scaling Concepts in Polymer Physics, Cornell University Press, New York, 1979.
[18] M.E. Cates, Reptation of living polymers: dynamics of entangled polymers in the presence of reversible chain-scission reactions, Macromolecules 20 (1987) 2289–2296, https://doi.org/10.1021/ma00175a038.
[19] M.E. Cates, Dynamics of living polymers and flexible surfactant micelles: scaling laws for dilution, J. Phys. Fr. 49 (1988) 1593–1600, https://doi.org/10.1051/jphys:019880049090159300.
[20] M.E. Cates, Nonlinear viscoelasticity of wormlike micelles (and other reversibly breakable polymers), J. Phys. Chem. 84 (1990) 371–375, https://doi.org/10.1021/j100364a063.
[21] M.E. Cates, S.M. Fielding, Rheology of giant micelles, Adv. Phys. 55 (2006) 799–879, https://doi.org/10.1080/00018730601082029.
[22] F. Kern, R. Zana, S.J. Candau, Rheological properties of semidilute and concentrated aqueous solutions of cetyltrimethylammonium chloride in the presence of sodium salicylate and sodium chloride, Langmuir 7 (1991) 1344–1351, https://doi.org/10.1021/la00055a010.
[23] F. Kern, P. Lemarechal, S.J. Candau, M.E. Cates, Rheological properties of semidilute and concentrated aqueous solutions of cetyltrimethylammonium bromide in the presence of potassium bromide, Langmuir 8 (1992) 437–440, https://doi.org/10.1021/la00038a020.
[24] A. Khatory, F. Kern, F. Lequeux, J. Appell, G. Porte, N. Morie, A. Ott, W. Urbach, Entangled versus multiconnected network of wormlike micelles, Langmuir 9 (1993) 933–939, https://doi.org/10.1021/la00028a010.
[25] A. Khatory, F. Lequeux, F. Kern, S.J. Candau, Linear and nonlinear viscoelasticity of semidilute solutions of wormlike micelles at high salt content, Langmuir 9 (1993) 1456–1464, https://doi.org/10.1021/la00030a005.
[26] M. Pleines, W. Kunz, T. Zemb, D. Banczédi, W. Fieber, Molecular factors governing the viscosity peak of giant micelles in the presence of salts and fragrances, J. Colloid Interface Sci. 537 (2019) 682–693, https://doi.org/10.1016/j.jcis.2018.11.072.
[27] K.D. Danov, P.A. Kralchevsky, R.D. Stanimirova, S.D. Stoyanov, J.L. Cook, I. P. Stott, Analytical modeling of micelle growth. 4. Molecular thermodynamics of wormlike micelles from ionic surfactants: theory vs. experiment, J. Colloid Interface Sci. 584 (2021) 561–581, https://doi.org/10.1016/j.jcis.2020.10.004.
[28] T.J. Drye, M.E.Cates Living, Living networks: the role of cross-links in entangled surfactant solutions, J. Chem. Phys. 96 (1992) 1367–1375, https://doi.org/10.1063/1.462172.
[29] F. Lequeux, Reptation of connected wormlike micelles, Europhys. Lett. 19 (1992) 675–681, https://doi.org/10.1209/0295-5075/19/8/003.
[30] J. Appell, G. Porte, A. Khatory, F. Kern, S. Candau, Static and dynamic properties of a network of wormlike surfactant micelles (cetylpyridinium chlorate in sodium chlorate brine, J. Phys. II EDP Sci. 2 (1992) 1045–1052, https://doi.org/10.1051/jp2:1992104.
[31] C. Oelschlaeger, P. Suwita, N. Willenbacher, Effect of counterion binding efficiency on structure and dynamics of wormlike micelles, Langmuir 26 (2010) 7045–7053, https://doi.org/10.1021/la9043705.
[32] A. Aït Ali, R. Makhloufi, Linear and nonlinear rheology of an aqueous concentrated system of cethyltrimethylammonium chloride and sodium salicylate, Phys. Rev. E 56 (1997) 4474–4478, https://doi.org/10.1103/PhysRevE.56.4474.
[33] I.A. Kadoma, C. Ylitalo, J.W. van Egmond, Structural transitions in wormlike micelles, Rheol. Acta 36 (1997) 1–12, https://doi.org/10.1007/BF00366719.
[34] G. Cl. Oelschlaeger, S.J. Waton, Candau, Rheological behavior of locally cylindrical micelles in relation to their overall morphology, Langmuir 19 (2003) 10495–10500, https://doi.org/10.1021/la035082u.
[35] M. Youssry, L. Coppola, E.F. Marques, I. Nicotera, Unravelling micellar structure and dynamics in an unusually extensive DDAB/bile salt catanionic solution by rheology and NMR-diffusometry, J. Colloid Interface Sci. 324 (2008) 192–198, https://doi.org/10.1016/j.jcis.2008.04.048.
[36] H. Yin, Y. Lin, J. Huang, Microstructures and rheological dynamics of viscoelastic solutions in a catanionic surfactant system, J. Colloid Interface Sci. 338 (2009) 177–183, https://doi.org/10.1016/j.jcis.2009.05.076.
[37] G. Porte, R. Gomati, O. El Haitdmy, J. Appell, J. Marignan, Morphological transformations of the primary surfactant structures in brine-rich mixtures of

ternary systems (surfactant/alcohol/brine), J. Phys. Chem. 90 (1986) 5746–5751, https://doi.org/10.1021/j100280a055.
[38] M. Monduzzi, U. Olsson, O. Söderman, Bicontinuous “micellar” solutions, Langmuir 9 (1993) 2914–2920, https://doi.org/10.1021/la00035a031.
[39] I. Harwigsson, O. Söderman, O. Regev, Diffusion and cryo-transmission electron microscopy studies of bicontinuous "micellar" solutions, Langmuir 10 (1994) 4731–4734, https://doi.org/10.1021/la00024a056.
[40] T. Kato, T. Terao, T. Seimiya, Intermicellar migration of surfactant molecules in entangled micellar solutions, Langmuir 10 (1994) 4468–4474, https://doi.org/10.1021/la00024a015.
[41] D. Danino, Y. Talmon, H. Levy, G. Beinert, R. Zana, Branched threadlike micelles in an aqueous solution of a trimeric surfactant, Science 269 (1995) 1420–1421, https://doi.org/10.1126/science.269.5229.1420.
[42] Z. Lin, Branched worm-like micelles and their networks, Langmuir 12 (1996) 1729–1737, https://doi.org/10.1021/la950570q.
[43] T. Kato, Surfactant self-diffusion and networks of wormlike micelles in concentrated solutions of nonionic surfactants, Prog. Colloid Polym. Sci. 100 (1996) 15–18, https://doi.org/10.1007/bfb0115744.
[44] F. Nilsson, O. Söderman, J. Reimer, Phase separation and aggregate-aggregate interactions in the C9G1/C10G1 β-alkyl glucosides/water system. A phase diagram and NMR self-diffusion study, Langmuir 14 (1998) 6396–6402, https://doi.org/10.1021/la980597k.
[45] A. Bernheim-Groswasser, R. Zana, Y. Talmon, Sphere-to-cylinder transition in aqueous micellar solution of a dimeric (Gemini) surfactant, J. Phys. Chem. B 104 (2000) 4005–4009, https://doi.org/10.1021/jp994301a.
[46] A. Bernheim-Groswasser, E. Wachtel, Y. Talmon, Micellar growth, network formation, and criticality in aqueous solutions of the nonionic surfactant $C_{12}E_5$, Langmuir 16 (2000) 4131–4140, https://doi.org/10.1021/la991231q.
[47] Z. Lin, B. Lu, J.L. Zakin, Y. Talmon, Y. Zheng, H.T. Davis, L.E. Scriven, Influence of surfactant concentration and counterion to surfactant ratio on rheology of wormlike micelles, J. Colloid Interface Sci. 239 (2001) 543–554, https://doi.org/10.1006/jcis.2001.7618.
[48] V. Croce, T. Cosgrove, G. Maitland, T. Hughes, G. Karlsson, Rheology, cryogenic transmission electron spectroscopy, and small-angle neutron scattering of highly viscoelastic wormlike micellar solutions, Langmuir 19 (2003) 8536–8541, https://doi.org/10.1021/la0345800.
[49] M.W. Liberatore, F. Nettesheim, P.A. Vasquez, M.E. Helgeson, N.J. Wagner, E. W. Kaler, L.P. Cook, L. Porcar, Y.T. Hu, Microstructure and shear rheology of entangled wormlike micelles in solution, J. Rheol. 53 (2009) 441–458, https://doi.org/10.1122/1.3072077.
[50] D. Danino, L. Abezgauz, I. Portnaya, N. Dan, From discs to ribbons networks: the second critical micelle concentration in nonionic sterol solutions, J. Phys. Chem. Lett. 7 (2016) 1434–1439, https://doi.org/10.1021/acs.jpclett.6b00266.
[51] T. Liu, Q. Lei, J. Dong, X. Li, Y. Lu, T. Zhou, Light-responsive vesicles based on azobenzene containing imidazolium surfactants and sodium oleate, Colloid Polym. Sci. 297 (2019) 1489–1497, https://doi.org/10.1007/s00396-019-04557-8.
[52] M.T. Georgiev, L.A. Aleksova, P.A. Kralchevsky, K.D. Danov, Phase separation of saturated micellar network and its potential applications for nanoemulsification, Colloids Surf. A 607 (2020), 125487, https://doi.org/10.1016/j.colsurfa.2020.125487.
[53] S.E. Anachkov, G.S. Georgieva, L. Abezgauz, D. Danino, P.A. Kralchevsky, Viscosity peak due to shape transition from wormlike to disklike micelles: effect of dodecanoic acid, Langmuir 34 (2018) 4897–4907, https://doi.org/10.1021/acs.langmuir.8b00421.
[54] K.D. Danov, G.M. Radulova, P.A. Kralchevsky, K. Golemanov, S.D. Stoyanov, Surface shear rheology of hydrophobin adsorption layers: Laws of viscoelastic behavior with applications to long-term foam stability, Faraday Discuss. 158 (2012) 195–212, https://doi.org/10.1039/c2fd20017a.
[55] R. Nagarajan, E. Ruckenstein, Theory of surfactant self-assembly: a predictive molecular thermodynamic approach, Langmuir 7 (1991) 2934–2969, https://doi.org/10.1021/la00060a012.
[56] K.D. Danov, P.A. Kralchevsky, S.D. Stoyanov, J.L. Cook, I.P. Stott, Analytical modeling of micelle growth. 1. Chain-conformation free energy of binary mixed spherical, wormlike and lamellar micelles, J. Colloid Interface Sci. 547 (2019) 245–255, https://doi.org/10.1016/j.jcis.2019.03.105.
[57] K.D. Danov, P.A. Kralchevsky, S.D. Stoyanov, J.L. Cook, I.P. Stott, Analytical modeling of micelle growth. 2. Molecular thermodynamics of mixed aggregates and scission energy in wormlike micelles, Colloid Interface Sci. 551 (2019) 227–241, https://doi.org/10.1016/j.jcis.2019.05.017.
[58] S. Różańska, Rheology of wormlike micelles in mixed solutions of cocoamidopropyl betaine and sodium dodecylbenzenesulfonate, Colloid Surf. A 482 (2015) 394–402, https://doi.org/10.1016/j.colsurfa.2015.06.045.
[59] G.S. Georgieva, S.E. Anachkov, I. Lieberwirth, K. Koinov, P.A. Kralchevsky, Synergistic growth of giant wormlike micelles in ternary mixed surfactant solutions: effect of octanoic acid, Langmuir 32 (2016) 12885–12893, https://doi.org/10.1021/acs.langmuir.6b03955.
[60] W.P. Cox, E.H. Merz, Correlation of dynamics and steady flow viscosities, J. Polym. Sci. A 28 (1958) 619–622, https://doi.org/10.1002/pol.1958.1202811812.
[61] R.B. Patel, M.R. Patel, S.D. Thakore, B.G. Patel, Nanoemulsion as a valuable nanostructure platform for pharmaceutical drug delivery, in: Nano-and Microscale Drug Delivery Systems, Elsevier, Amsterdam, 2017, pp. 321–341, Chapter 17. https://doi.org/10.1016/B978–0-323–52727-9.00017–0.
[62] T.T.L. Nguyen, N. Anton, T.F. Vandamme, Oral pellets loaded with nanoemulsions, in: Nanostructures for Oral Medicine, Elsevier, Amsterdam, 2017, pp. 203–230, Chapter 8. https://doi.org/10.1016/B978–0-323–47720-8.00009–2.
[63] C. Chircov, A.M. Grumezescu, Nanoemulsion preparation, characterization, and application in the field of biomedicine, in: Nanoarchitectonics in Biomedicine, Elsevier, Amsterdam, 2019, pp. 169–188, Chapter 6. https://doi.org/10.1016/B978–0-12–816200-2.00019–0.
[64] S.A. Rogers, M.A. Calabrese, N.J. Wagner, Rheology of branched wormlike micelles, Curr. Opin. Colloid Interface Sci. 19 (2014) 530–535, https://doi.org/10.1016/j.cocis.2014.10.006.

Supplementary Material

for the article

Rheology of saturated micellar networks: Wormlike micellar solutions vs. bicontinuous micellar phases

Authors: T.N. Stancheva, M.T. Georgiev, G.M. Radulova, K.D. Danov, K.G. Marinova

Here, the reference numbers are different from those in the main text; the list of cited references is given at the end of the present Supplementary Material.

Appendix A. Phase behavior of 1:1 w/w SLES:CAPB solutions in the presence of salt

The structural chemical formulas of sodium laurylethersulfate and laurylamidopropyl betaine are given in Fig. A1. We used sodium laurylethersulfate with one ethylene oxide group (SLES) and cocamidopropyl betaine (CAPB). All mixed surfactant solutions are with a fixed 1:1 weight ratio of ionic and zwitterion surfactants at total concentration C_{tot}. The used CAPB sample contains admixture of NaCl. Thus the base SLES+CAPB solutions contain different amounts of Na^+ and Cl^- ions because of the SLES dissociation and the admixture of NaCl in the CAPB sample (see Table A1). For more details see the main text.

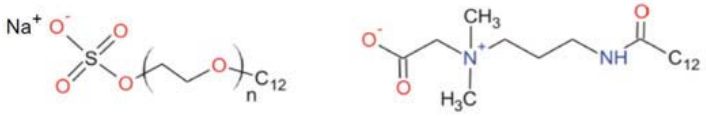

sodium laurylethersulfate laurylamidopropyl betaine

Fig. A1. Structural chemical formulas of sodium laurylethersulfate and laurylamidopropyl betaine.

Table A1. Total concentrations of Na^+ and Cl^- ions in the solutions of 1:1 w/w SLES:CAPB.

C_{tot}	3 wt%	5 wt%	8 wt%	10 wt%	12 wt%	14 wt%
Na^+ (mM)	95	158	253	316	379	443
Cl^- (mM)	50	83	133	166	199	232

Figs. A2–A7 show photographs of 1:1 w/w SLES:CAPB solutions for different total surfactant concentrations, C_{tot}, and different amounts of added $MgCl_2$. The concentration of added salt is C_{salt} and the minimal salt concentration, above which the bicontinuous micellar phase is observed, is C_{sep}.

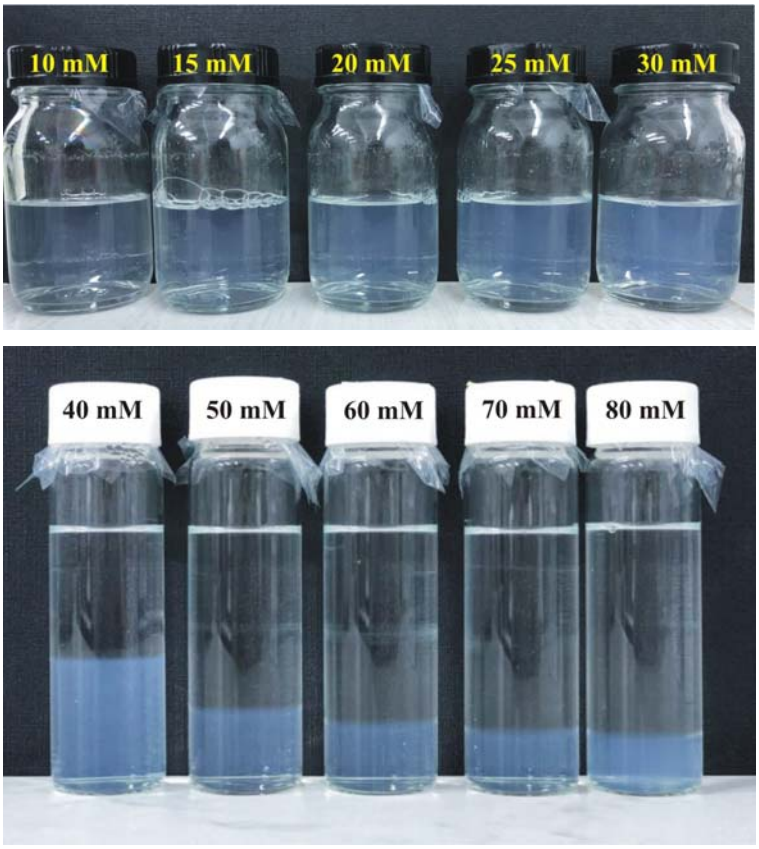

Fig. A2. Photographs illustrating the phase behavior of 3 wt% 1:1 w/w SLES:CAPB solutions with the rise of added salt concentration. The concentration of $MgCl_2$ is given on the caps of the vails. C_{sep} > 30 mM.

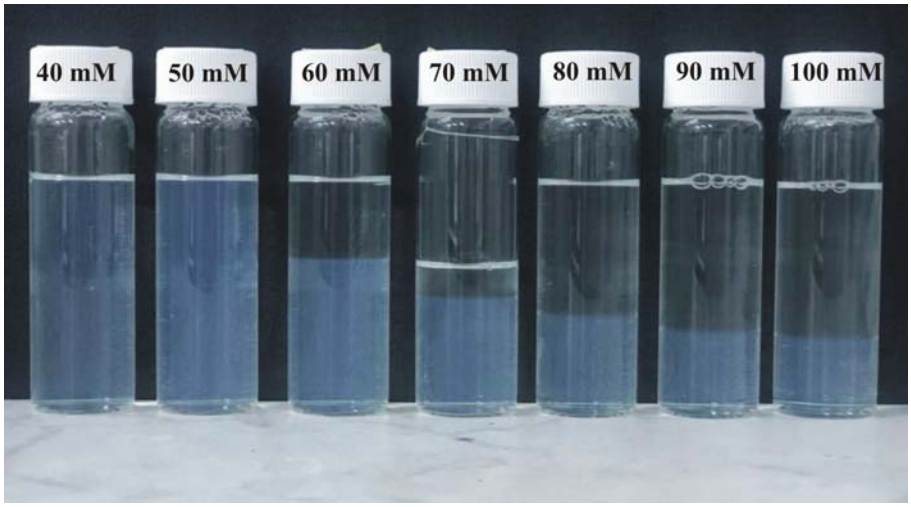

Fig. A3. Photographs illustrating the phase behavior of 5 wt% 1:1 w/w SLES:CAPB solutions with the rise of added salt concentration. The concentration of $MgCl_2$ is given on the caps of the vails. C_{sep} > 50 mM.

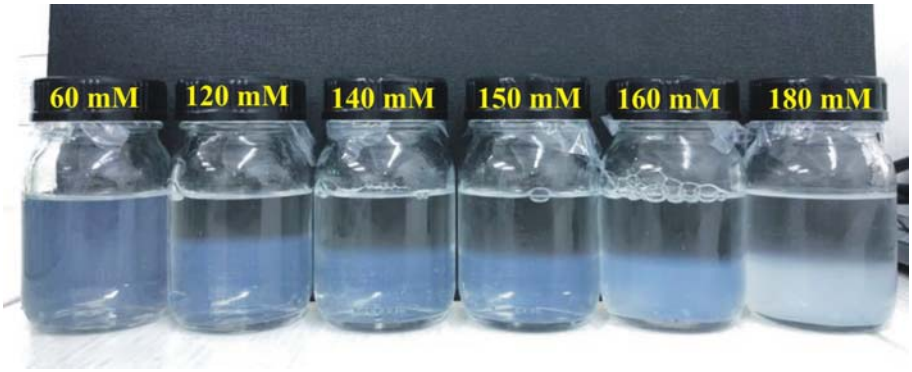

Fig. A4. C_{tot} = 8 wt% in the presence of $MgCl_2$. C_{sep} > 60 mM.

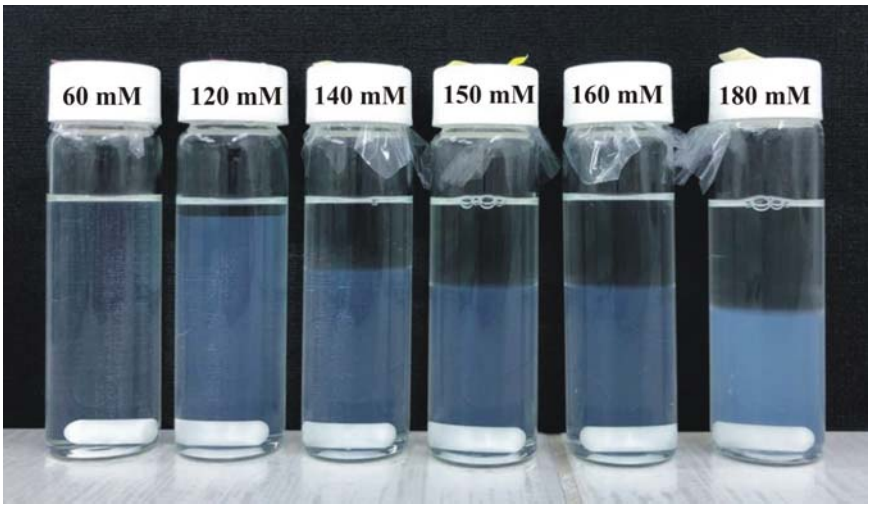

Fig. A5. C_{tot} = 10 wt% in the presence of $MgCl_2$. $C_{sep} \approx$ 120 mM.

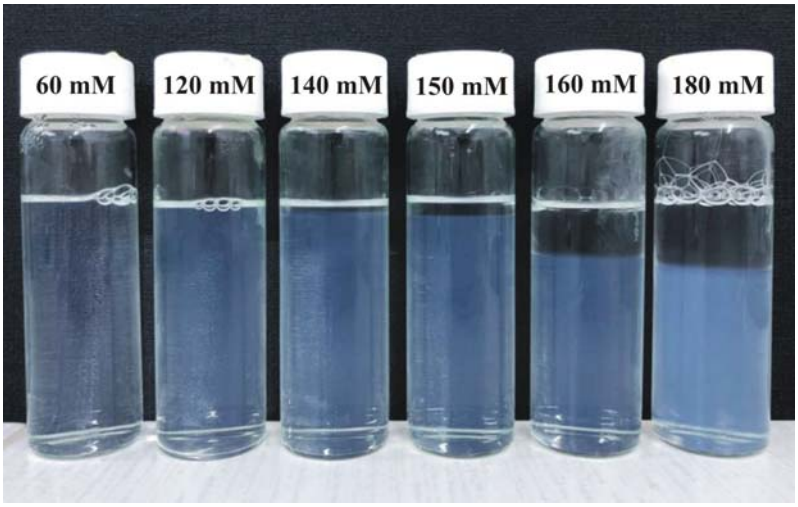

Fig. A6. C_{tot} = 12 wt% in the presence of $MgCl_2$. $C_{sep} \approx$ 140 mM.

Fig. A7. C_{tot} = 14 wt% in the presence of $MgCl_2$. $C_{sep} \approx$ 160 mM.

Analogous phase behavior is observed in the case of added $MgSO_4$, see Fig. A8 and Ref. [1]. The obtained values of C_{sep} in the case of $MgSO_4$ are slightly higher than those in the presence of added $MgCl_2$.

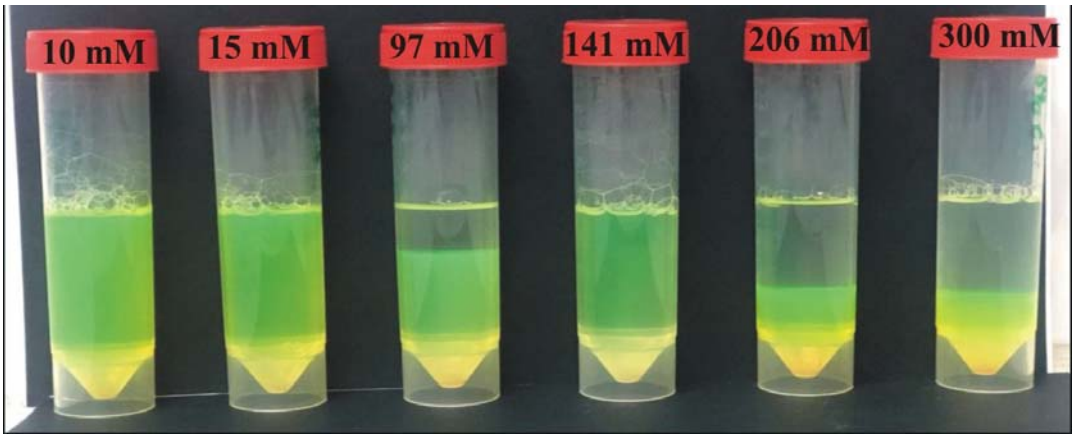

Fig. A8. Photographs illustrating the phase behavior of 5 wt% 1:1 w/w SLES:CAPB solutions with the rise of added $MgSO_4$ concentration. The concentration of $MgSO_4$ is given on the caps of the vails. C_{sep} is below 97 mM.

For C_{salt} > 200 mM, the solutions contain crystals because of the salting-out effect [1]. Indeed, Fig. A9 shows the micrographs of 5 wt% solutions after preparation in the case of added $MgSO_4$ for C_{salt} = 97 and 206 mM. It is well illustrated that for C_{salt} = 97 mM (left graph), the solution contains droplets from saturated micellar network, while in the case of 206 mM added $MgSO_4$ (right graph), the solution contains crystals, which coexist with the multiconnected micellar phase. The crystal formation is observed for all studied surfactant concentrations at large enough added salt concentration.

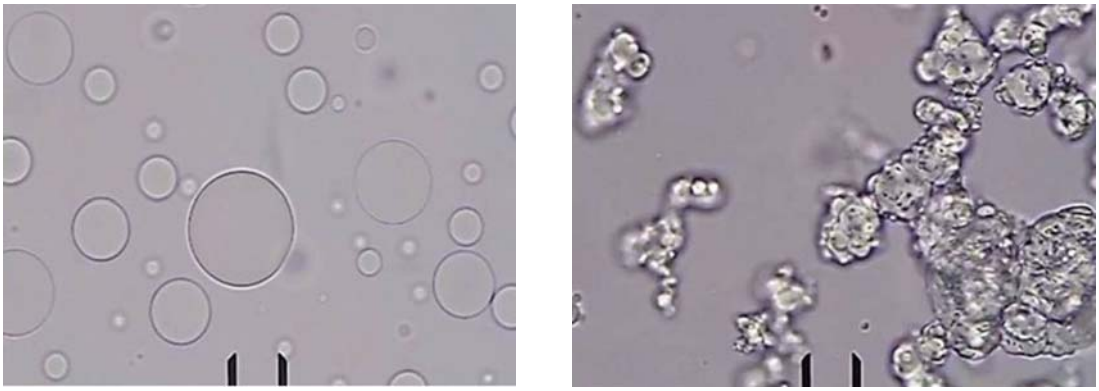

Fig. A9. Micrographs of 5 wt% 1:1 w/w SLES:CAPB solutions in the presence of 97 mM $MgSO_4$ (left graph) and 206 mM $MgSO_4$ (right graph). The marks correspond to 20 μm.

Appendix B. Geometry of the working elements of the rheometer

The schemes of the used working elements of the rheometer are given in Fig. B1.

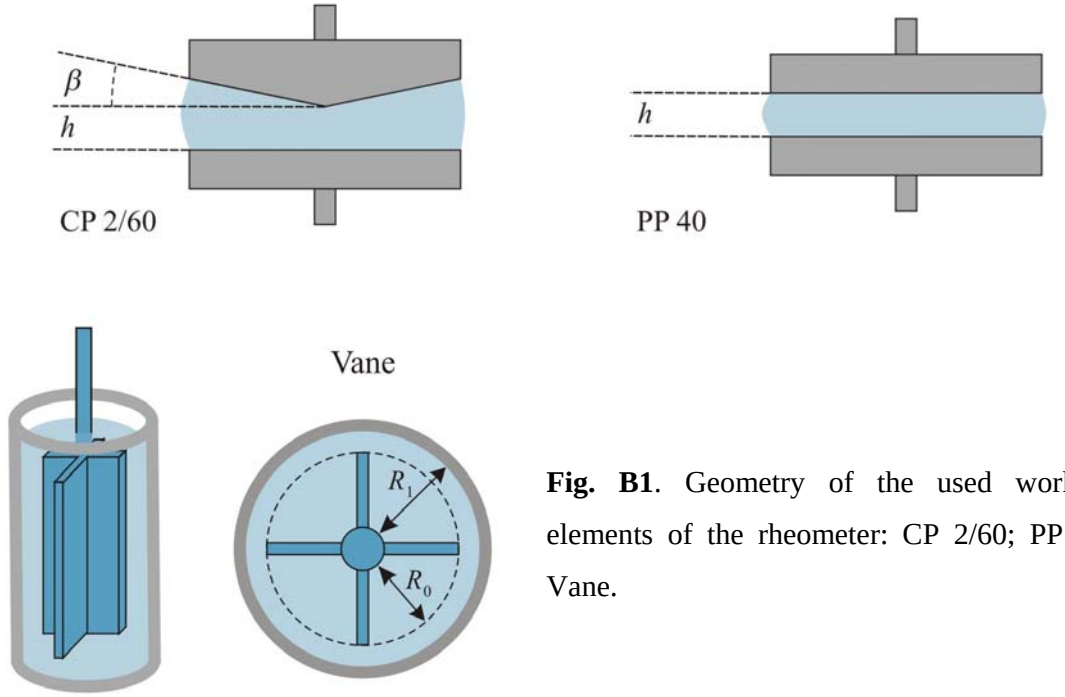

Fig. B1. Geometry of the used working elements of the rheometer: CP 2/60; PP 40; Vane.

CP 2/60 element is with a cone-and-plate geometry: cone angle $\beta = 2^o$; minimal gap distance h = 70 μm; disk diameter 60 mm. PP 40 element realizes a plane parallel geometry: gap distance h = 1 mm; disk diameter 40 mm. The Vane element ensures a slippage of the boundary layer around the rotational element: vane radius R_0 = 25 mm; outer radius R_1 = 28 mm; thickness of the active shearing zone $R_1 - R_0$ = 3 mm. All systematic experiments were performed with element CP 2/60.

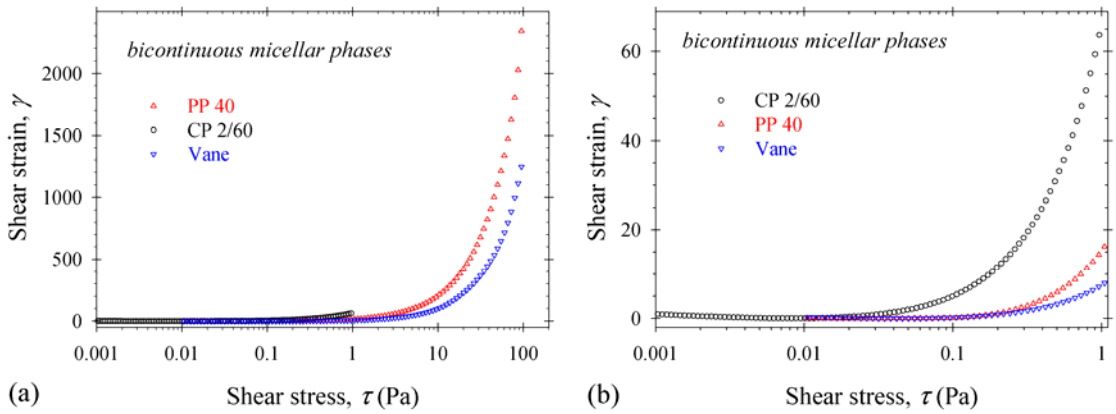

Fig. B2. Comparison between the shear strains, γ, vs. shear stresses, τ, measured in the stress-ramp regime for isolated bicontinuous micellar phases using different working elements of the rheometer: (a) the increase of the shear stress to 100 Pa; (b) enlarged view for $\tau < 1$ Pa.

In order to measure the yield stress of the isolated BMPs, the shear strains, γ, versus shear stresses, τ, were measured in the stress-ramp regime (Fig. B2). One sees the considerable difference between the measured dependencies. At low shear stresses, the shear strains in the case of CP 2/60 are the highest (Fig. B2b), while for large shear stresses, the data for γ in the case of PP 40 have the largest values. At each applied shear stress τ, the shear strains are accumulated from the previous stages, so that γ depends on the prehistory of the experimental conditions. The invariant rheological properties are the apparent viscosities for a given shear stress (see Figs. 9 and 10 in the main text).

Appendix C. Typical dependencies of the apparent viscosity on the shear rate

The typical dependencies of the apparent viscosity, η, on the shear rate, $\dot{\gamma} \equiv \mathrm{d}\gamma / \mathrm{d}t$, measured in the steady-shear regime for different micellar structures are illustrated in Figs. 1a and 1b in the case of added $MgCl_2$ and in Fig. C1 in the case of added $MgSO_4$. One sees that for C_{salt} = 10 and 206 mM, the Newtonian viscosity, η_∞, is well defined at large shear rates, but the zero-shear viscosity, η_0, cannot be determined (Figs. C1a and C1d). For these micellar solutions, we used the most probable value of the apparent viscosity at shear rate 0.01 s^{-1}, $\eta_{0.01}$. In contrast, for the solutions with wormlike and branched micelles (Figs. C1b and C1c), the zero-shear viscosity is observed, but the shear thinning behavior takes place for shear rates up to 100 s^{-1}. In this case, we used the most probable value of η at high shear rates 100 s^{-1}, that is η_{100}. All power law indexes are around 1.

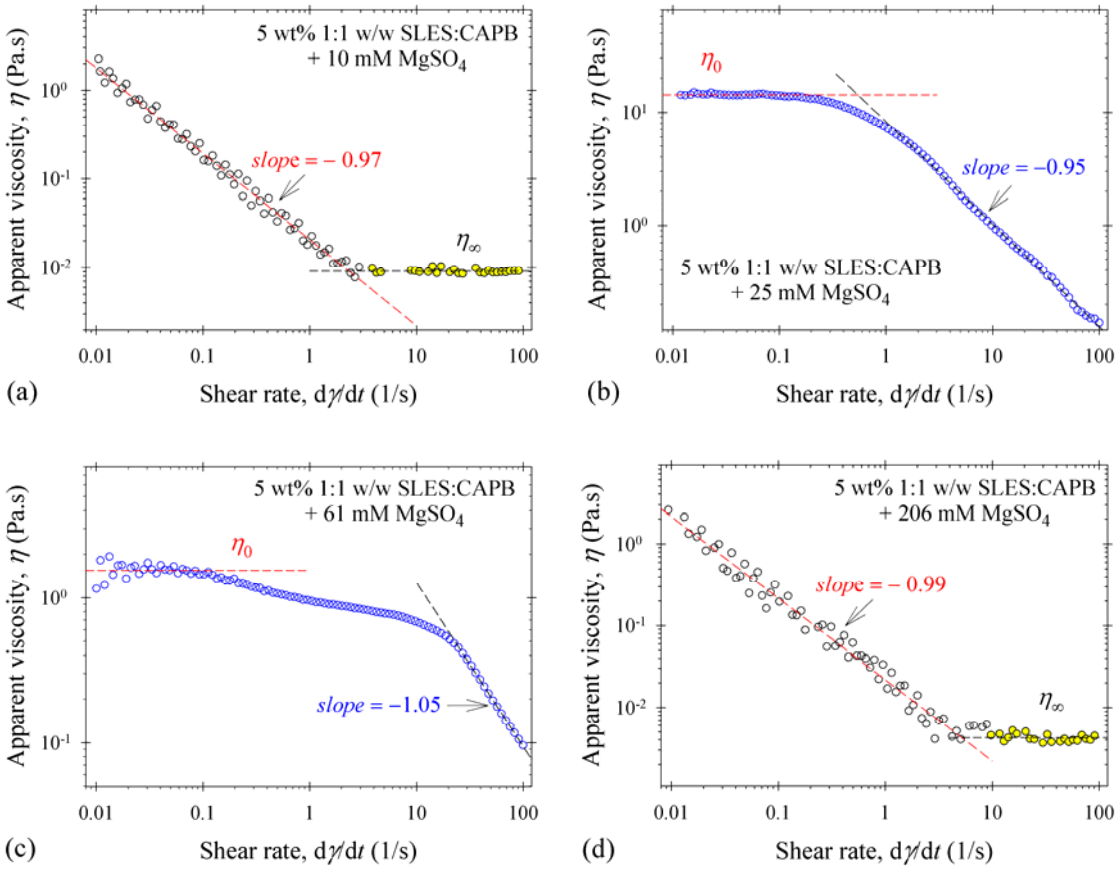

Fig. C1. Typical flow curves for C_{tot} = 5 wt% and different concentrations of added $MgSO_4$: (a) C_{salt} = 10 mM; (b) C_{salt} = 25 mM; (c) C_{salt} = 61 mM; (d) C_{salt} = 206 mM.

The dependence of the experimental viscosities, η_0, $\eta_{0.01}$, η_{100}, and η_∞, on the concentration of added $MgCl_2$ for total surfactant concentrations 8, 10, 12, and 14 wt% are summarizes in Figs. 4a and 4b. The respective data are obtained from the experimental flow curves like those illustrated in Figs. 1a, 1b, C1, and C2. For example, Fig. C2a shows that the zero-shear viscosity is measured with a good precision even at low C_{salt} = 10 mM $MgCl_2$ for surfactant concentrations above 5 wt%. This result is explained with the increase of the ionic strength of the mixed surfactant solutions because of the dissociation of SLES and the amount of NaCl in the CAPB sample (see Table A1) [2]. As can be expected (Fig. C2b), the solutions with added 20 mM $MgCl_2$ contain wormlike micelles for all studied surfactant concentrations, $C_{tot} \geq 5$ wt%. The lower zero-shear viscosities are also well measured in the case of branched micellar solutions (Fig. C2c).

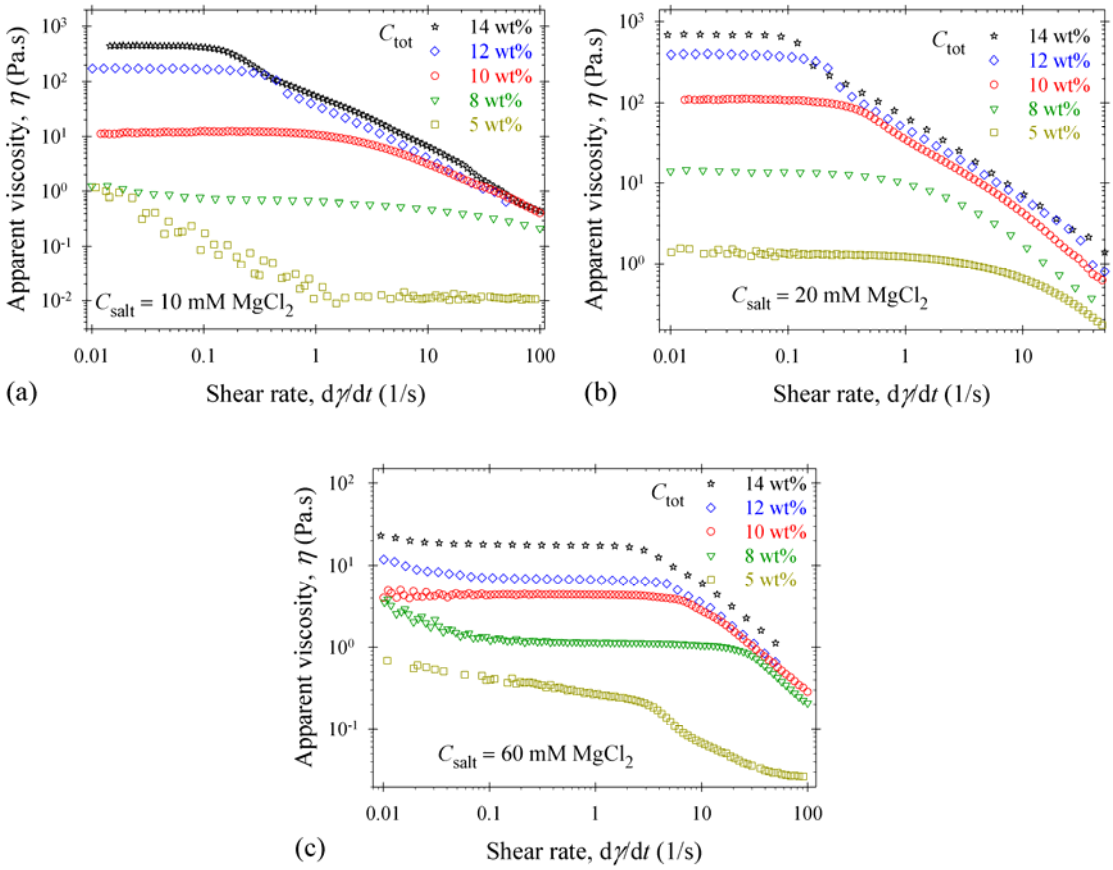

Fig. C2. Typical flow curves for different surfactant concentrations, C_{tot}, and different concentrations of added $MgCl_2$: (a) C_{salt} = 10 mM; (b) C_{salt} = 20 mM; (c) C_{salt} = 60 mM.

Appendix D. Storage and loss moduli from oscillatory regime

The dependencies of the storage, G', and loss, G'', moduli on the amplitude of oscillations, γ_a, are shown in Fig. D1 and Fig. 1d. For different surfactant concentrations in the presence of 20 mM $MgCl_2$, the moduli have constant values up to $\gamma_a = 0.5$ for G' and up to $\gamma_a = 0.1$ for G''. Therefore, the linear regime with respect to the amplitudes of oscillations takes place for $\gamma_a < 0.1$. In all oscillatory experiments, we checked the linearity and performed oscillatory experiments with low enough amplitude, $\gamma_a = 0.02$.

There are two parameters in the Maxwell equations, Eq. (1): elasticity G_0; relaxation time τ_R. The dependencies of the storage and loss moduli, G' and G'', on the frequency, ω, give the possibility to obtain them in the range of constant elasticity and viscosity of the solutions. Fig. D2 shows the experimental data for $G'(\omega)$ and $G''(\omega)$ for wormlike micellar solutions (C_{tot} = 10, 12, and 14 wt% and C_{salt} = 20 mM $MgCl_2$). The solid lines correspond to the best fit using the Maxwell rheological model with constant values of G_0 and τ_R.

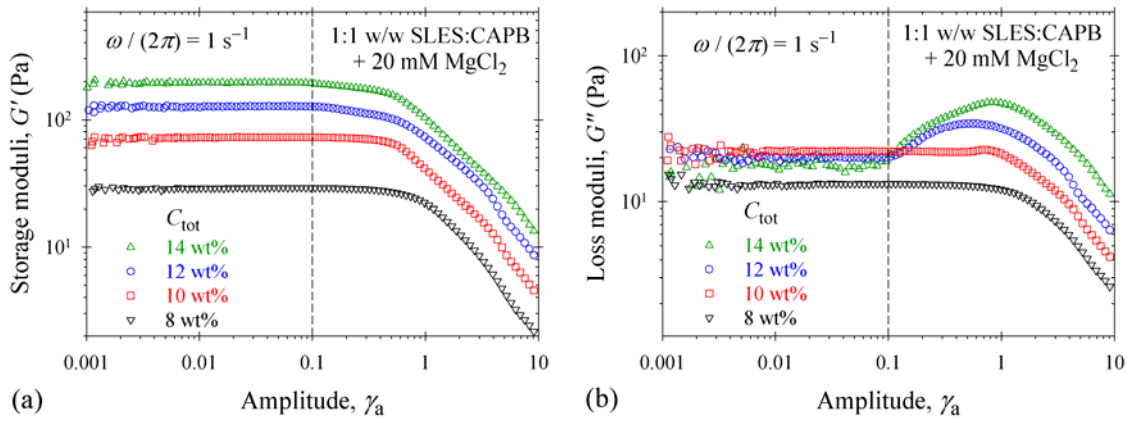

Fig. D1. Storage (a) and loss (b) moduli obtained from oscillatory experiments vs. amplitude of oscillations at frequency 1 Hz. The solutions contain 20 mM $MgCl_2$ and C_{tot} = 8, 10, 12, and 14 wt%.

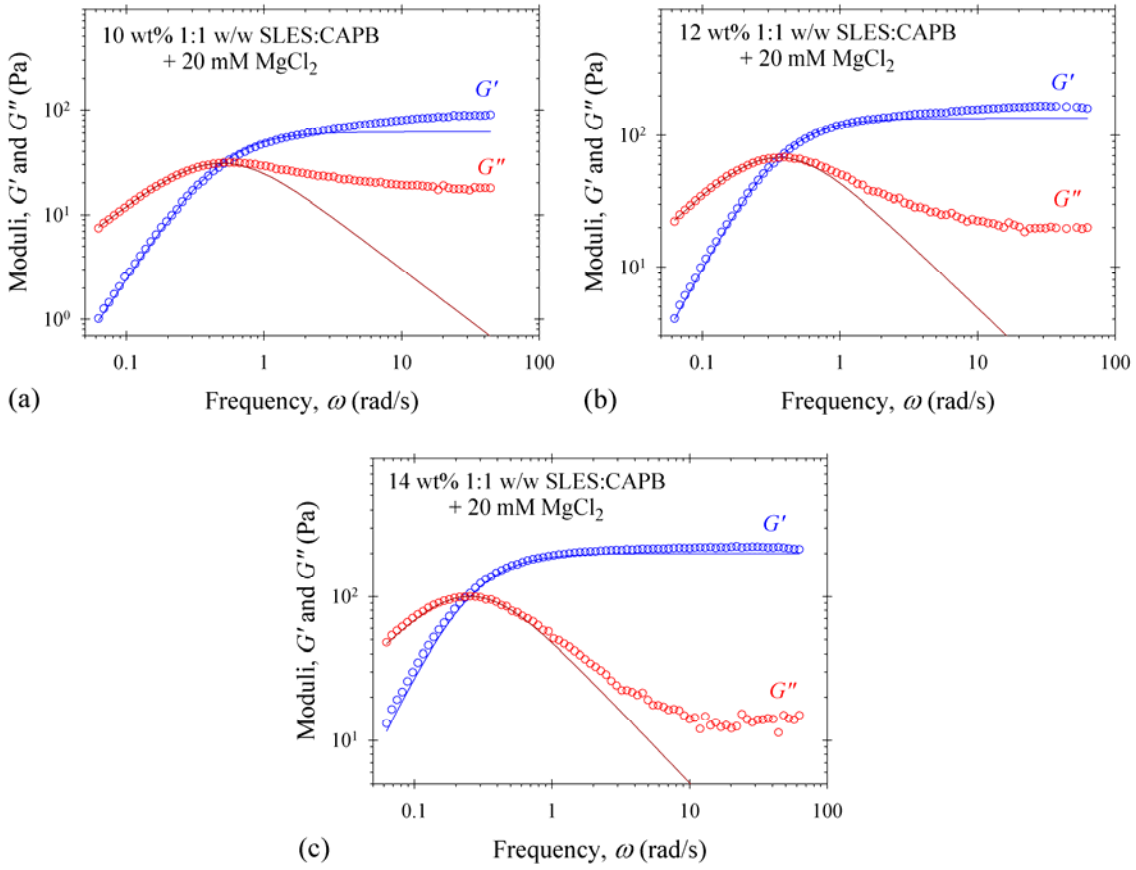

Fig. D2. Storage and loss moduli vs. frequency of oscillations for solutions containing 20 mM $MgCl_2$: (a) C_{tot} = 10 wt%; (b) C_{tot} = 12 wt%; (c) C_{tot} = 14 wt%. The solid lines correspond to the best fit using the Maxwell equations.

The raw data for the storage and loss moduli versus frequency obtained for C_{tot} = 8 wt% and C_{salt} = 20 mM $MgCl_2$ are shown in Fig. D3a. One sees the excellent reproducibility of measurements from two independent runs. These data deviate considerably from the Maxwell model and should be processed using the augmented version of the Maxwell model [2]. The characteristic frequency $<\nu_{ch}> \equiv G''\omega / G'$ obeys Eq. (3) in the main text. The solid line in Fig. D3b corresponds to the best fit of experimental data using Eq. (3).

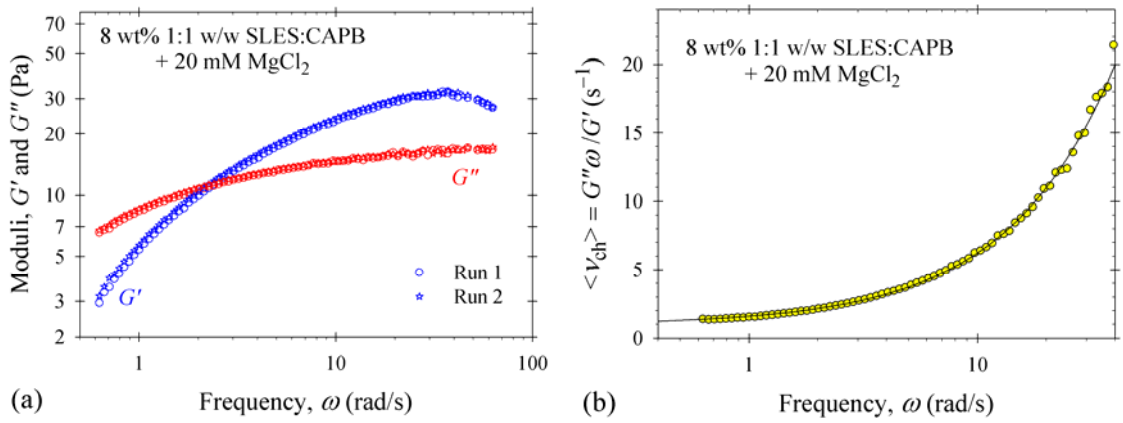

Fig. D3. (a) Storage and loss moduli vs. frequency of oscillations for 8 wt% surfactant solution containing 20 mM $MgCl_2$. (b) Dependence of the characteristic frequency $<\nu_{ch}>$ on ω – the solid line is the best fit using Eq. (3).

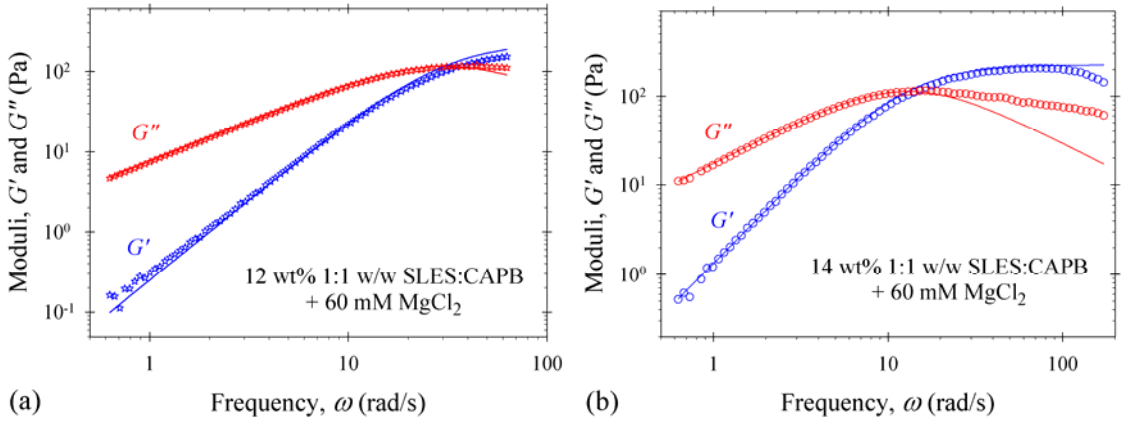

Fig. D4. Storage and loss moduli vs. frequency for branched micellar solutions containing 60 mM $MgCl_2$: (a) C_{tot} = 12 wt%; (b) C_{tot} = 14 wt%. The solid lines correspond to the best fits according to the Maxwell model.

In the case of branched micelles (C_{salt} = 60 mM $MgCl_2$) and relatively high surfactant concentrations (C_{tot} = 10, 12, and 14 wt%), the moduli $G'(\omega)$ and $G''(\omega)$ obey the Maxwell

equations for frequencies of oscillations lower than 30 rad/s (Fig. D4). The non-typical deviations from the Cole-Cole plots are illustrated in Fig. 6a.

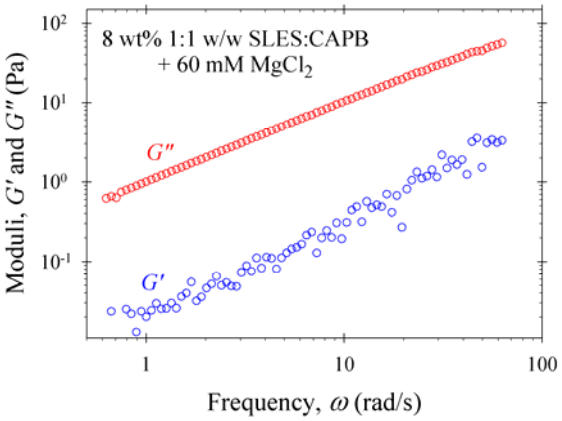

Fig. D5. Storage and loss moduli vs. frequency for branched micellar solutions at total surfactant concentration 8 wt% in the presence of 60 mM $MgCl_2$.

For lower surfactant concentrations (8 wt%), the values of the loss moduli are more than 20 times greater than those for the storage moduli in the range of the studied frequencies. For that reason only the viscosity of this solution can be calculated with good precision (see Fig. 6b).

Appendix E. Rheology of bicontinuous micellar phases

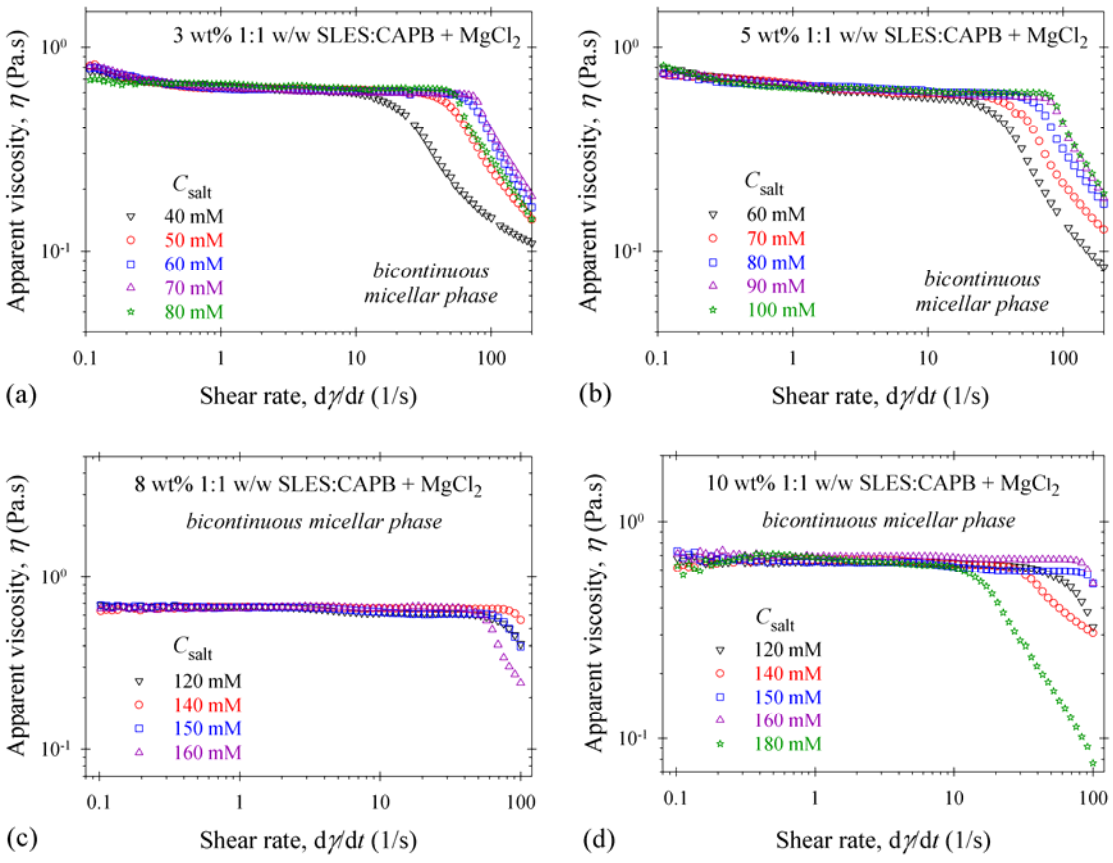

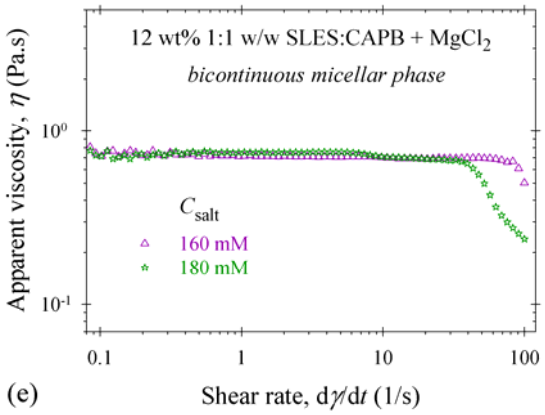

Fig. E1. Rheological properties of isolated BMPs in the steady-shear regime for different surfactant and salt concentrations: (a) C_{tot} = 3 wt%; (b) C_{tot} = 5 wt%; (c) C_{tot} = 8 wt%; (d) C_{tot} = 10 wt%; (e) C_{tot} = 12 wt%.

Fig. E1 summarizes experimental data for the apparent viscosity measured in the shear-ramp regime for bicontinuous micellar phases (BMP) isolated from the surfactant solutions at concentrations 3 wt% ≤ C_{tot} ≤ 12 wt% in the presence of different amount of $MgCl_2$. One sees that the zero-shear viscosities of all BMP are approximately constant and η_0 = 0.66 Pa.s. The transitions to the shear-thinning-rheological behavior take place at different shear rates depending on C_{tot} and C_{salt}.

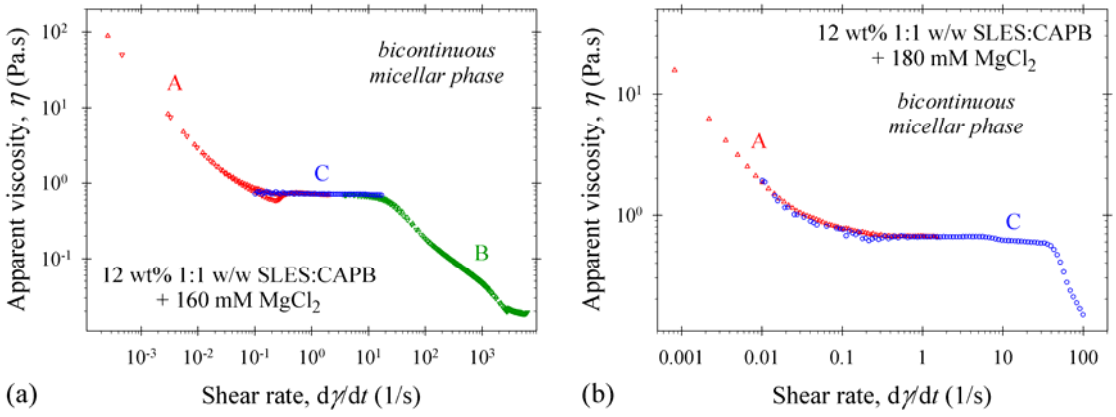

Fig. E2. Rheological behavior of the BMPs in different regimes. 12 wt% surfactant solutions with added different amount of salt: (a) η vs. shear rate in the stress-ramp regime (A and B) and in the steady-shear regime (C), C_{salt} = 160 mM $MgCl_2$; (b) η vs. shear rate in the stress-ramp regime (A) and in the steady-shear regime (C), C_{salt} = 180 mM $MgCl_2$.

Fig. E2 shows the dependence of the apparent viscosity on the shear rate measured for BMPs isolated from 12 wt% surfactant solutions in the presence of 160 and 180 mM $MgCl_2$.

The experimental curves A and B are obtained in the stress-ramp regime and the flow curves C – in the steady-shear regime. One sees that regimes A→C→B match in the frame of experimental errors. These data are used in Fig. 9b to calculate the yield stress of the bicontinuous micellar phase.

References

[1] M.T. Georgiev, L.A. Aleksova, P.A. Kralchevsky, K.D. Danov, Phase separation of saturated micellar network and its potential applications for nanoemulsification, Colloids Surf. A 607 (2020) 125487.

[2] V.I. Yavrukova, G.M. Radulova, K.D. Danov, P.A. Kralchevsky, H. Xu, Y.W. Ung, J.T. Petkov, Rheology of mixed solutions of sulfonated methyl esters and betaine in relation to the growth of giant micelles and shampoo applications, Adv. Colloid Interf. Sci. 275 (2020) 102062.